UNIVERSITY POLITEHNICA of BUCHAREST, ROMANIA
THE FACULTY OF APPLIED SCIENCES

DOCTORAL THESIS SUMMARY

OPTICAL AND ELECTRONIC PHENOMENA IN SEMICONDUCTOR NANOSTRUCTURES

FENOMENE OPTICE ȘI ELECTRONICE ÎN NANOSTRUCTURI SEMICONDUCTOARE

PH.D student: **Cristina - Ramona PUIU (TRUȘCĂ)**

COMISIA DE DOCTORAT

President	**Prof. Dr. Cristina STAN**	from	University *"Politehnica"* Bucharest
Supervisor	**Prof. Dr. Ecaterina Cornelia NICULESCU**	from	University "*Politehnica"* Bucharest
Member	**Prof. Dr. Adrian RADU**	from	Univ. "*Politehnica"* Bucharest
Member	**Prof. Dr. Petru – Edward NICA**	from	Univ. *Tehnică "Gheorghe Asachi* "Iași
Member	**Prof. Dr. Liviu LEONTIE**	from	Univ. "*Alexandru Ioan Cuza*" Iași

BUCHAREST, 2021

Thanks

I would like to thank all those who gave me their support and scientific support in the development and writing of the thesis, as well as all those who supported me morally and without whom, sometimes, the reason to go further is hard to find.

The scientific substantiation and the elaboration of this doctoral thesis would have been impossible without the help, support and guidance of special people who, through high professional degree and dedication, contributed to my professional training, instilling in me the courage to go further.

Special gratitude and chosen thanks to Prof. Dr. Ecaterina Cornelia Niculescu (scientific leader), for the trust given, for the scientific guidance, patience and professionalism, support, coordination and full understanding shown throughout the training process and writing the doctoral thesis. Thank you for agreeing to share with me your rich experience gained over the years of study, and without your support I would not have been able to complete this thesis.

Special gratitude I owe to the members of the steering committee: prof. Dr. Cristina Stan, prof. Dr. Mona Mihăilescu, prof.dr. Mihail Cristea, for the precious time given, for the valuable scientific advice, as well as for the competent and permanent guidance during the elaboration and realization of this doctoral thesis.

Thanks to the distinguished referents from the doctoral commission, composed of prof. Dr. Adrian Radu, prof.dr. Petru-Edward Nica and prof. Dr. Liviu Leonte for the time given and the patience with which they analyzed this paper as well as for the valuable scientific advice.

Completing the doctoral thesis would not have been possible without the help and constant support of my husband who trusted me and was with me unconditionally.

Last but not least, I would like to express my sincere thanks to the family for the love, understanding and moral support provided during these years, giving me the motivation and conditions necessary to complete and complete my doctoral thesis.

Thank you to all those who, directly or indirectly, helped me and supported me during these years in which I developed this work.

Contents

KEYWORDS: semiconductor, quantum rings, quantum dot ,semi-parabolic quantum well, non-resonant intense laser, static electric field, magnetic field, electromagnetically induced transparency , dome-shaped quantum dot; non-linear optical property; hydrogenic donor, wetting layer, donor impurity, diamagnetic susceptibility, disc shape quantum dot, Stark effect, polarizability, oscillator strength.

NOTE: The summary keeps the same numbering of chapters, subchapters, figures, tables, including bibliographic references as in the doctoral thesis.

Chapter 1

Introduction

Studies related to the effects of an electromagnetic field on quantum nanostructures under the influence of static external fields - electric or magnetic - are a field of considerable scientific interest. The interaction of external fields with electrons in quantum heterostructures has led to the emergence of interesting and potentially beneficial effects, such as phenomena of nonlinear optics, electromagnetically induced transparency, the Stark effect of quantum confinement, etc. The interest lies in the fact that by choosing the size, shape and constituent materials it is possible to modulate and optimize the optical properties, allowing their use in devices such as LEDs, detectors, lasers, modulators and optical switches.

The design of these devices requires different properties of quantum heterostructures to be studied, such as: refractive index, optical absorption coefficient, probabilities of transition between bands, Stark displacement, etc. On the other hand, it is convenient to modify the properties by external disturbances, so as to obtain nanostructures with operating frequencies required in practical applications and the presence of static fields, -electric and magnetic-, pressure and temperature change or the action of a laser radiation of high - intensity offer this possibility. Moreover, during the growth process it is possible, intentionally or unintentionally, to add impurities to nanostructures, significantly affecting the optical and transport properties and leading to new transitions in optoelectronic devices.

This brief exposition of the possibility of using nanostructures in light detection, emission and absorption devices, a possibility based on their remarkable optical properties, motivates the choice of the topic and objectives of the thesis. From the wide range of systems studied in the literature, two types of nanostructures are promising for high-performance semiconductor devices. These are (i) quantum rings (QRs) with or without impurities and (ii) self-assembled quantum dots (QDs) from III-V semiconductors and their alloys.

In this thesis, theoretical studies on these particular cases of nanostructures and specific characteristics induced by external disturbances are presented. Thus, we investigated the possibility of inducing optical transparency in semiparabolic quantum wells and in GaAs quantum rings in the presence of a control and a sample laser. The phenomenon creating a spectral region of transparency inside a sample radiation absorption line, due to a destructive quantum interference resulting from two transitions in a three-level system. The analysis of some external fields effects and of the presence of a donor impurity on the position and width of the transparency window and of the group speed in nanostructures is of special interest.

The modification of the optical properties of semiconductor heterostructures in response to the application of an electric fields application consists of shifts of the spectral lines towards higher or lower energies and the modification of the intensity of the absorption maximums.

Interesting effects occur in asymmetric quantum structures, with structural asymmetry generated either by the presence of impurities (e.g., a noncentric donor in a concentric QR),

or from the geometry of the confinement potential, as in self-assembled quantum dots with residual layer. In such structures -studied in the thesis- the applied electric field can change the asymmetry of the potential. As a result, the energy spectrum and wave functions associated with the electrons depend significantly on the direction of the field (due to the polarization of the field-induced spatial charge distribution) and high values can be obtained for second-order nonlinear susceptibility.

Because it can be applied experimentally in a well-controlled way, the magnetic field is an interesting tool to control and modulate the output intensity of optoelectronic devices. Many studies have been reported on electronic properties, as well as on linear and nonlinear optical absorption of QDs induced by external magnetic fields.

However, the effect of applying a magnetic field on the electronic structure of a donor impurity and the associated optical transitions in QR and QD self-assembled with residual layer is little investigated and the thesis presented completes the studies related to this topic.

As objectives, this paper aims to study:

- electronic and optical properties of zero-dimensional nanostructures - quantum rings and self-assembled quantum dots with residual layer.
- the possibility of adjusting them by an adequate modification of the external fields- electric, magnetic, non-resonant laser radiation of high intensity - but also by the asymmetry of the confinement potential, obtained by geometry or by the presence and the position of impurity atoms.

The doctoral thesis entitled "OPTICAL AND ELECTRONIC PHENOMENA IN SEMICONDUCTOR NANOSTRUCTURES" comprises seven chapters.

The first chapter entitled **"Introduction"** briefly describes the importance of nanostructures studied from the point of view of fundamental physics, but also the possibility of their use in the construction of opto-electronic devices. The research objectives and the structure of the doctoral thesis are also presented.

Chapter 2 entitled **"Electronic states in nanostructures. General theoretical framework"** presents general aspects and a synthesis of the results recently published in the literature on the structure and properties of investigated nanostructures. The main theoretical notions that allow the modeling of the behavior of semiconductor quantum systems are presented: the theory of effective mass, the theory of optical absorption, numerical methods for solving the Schrödinger equation for zero-dimensional structures under the action of external perturbations. The last part of the chapter contains a study of literature related to electro-optical phenomena in nanostructures, focusing on the phenomenon of electromagnetically induced transparency and the description of the behavior of quantum rings in GaAs / AlGaAs and self-assembled quantum points in InAs / GaAs in electric fields and magnetic fields.

The following four chapters constitute the original contributions to the chosen field, namely:

Chapter 3 entitled **"Effects of electric, magnetic and intense laser fields on the electromagnetically induced transparency in a semi-parabolic quantum well"** describe the achievement of an optimum of the characteristics of induced transparency through an appropriate choice of applied external fields.

Chapter 4 entitled **"Magnetic field control of absorption coefficient and group index in an impurity doped quantum disc"**studies the electronic properties and optical characteristics - absorption coefficient, refractive index and group index - for a disk quantum with a hydrogen impurity under the action of a magnetic field.

Chapter 5 entitled **"Stark shift and oscillator strenghts in a GaAs quantum ring with off-center donor impurity "** presents a theoretical study of the Stark effect in a GaAs quantum ring under the action of a radial electric field. The results obtained in the approximation of the effective mass show that for moderate electric field intensities, Stark displacement is linearly dependent on electric field strength, while oscillator strength associated with optical transitions is strongly dependent on incident light polarization and impurity position.

Chapter 6 entitled **"Magnetic-field dependence of the impurity states in a dome-shaped quantum dot"** studies the electronic states associated with a donor impurity and the corresponding transition energies at a quantum point in InAs / GaAs coupled with a residual layer under the action of a magnetic field.

Chapter 7 entitled **"Optical non-linearities associated to hydrogenic impurities in InAs/GaAs self-assembled quantum dots under applied electric fields"** describes the effects of a hydrogen impurity on nonlinear optical processes at a quantum point with residual layer of InAs / GaAs, under the action an electric field applied perpendicular to the residual layer.

Each of chapters 3-7 concludes with conclusions, which point out the elements of originality of the thesis.

The paper ends with the chapter in which the main Conclusions and perspectives are highlighted as well as the List of publications - results of the research carried out during the doctoral studies.

Chapter 2

Electronic states in nanostructures. General theoretical framework

Chapter 2 presents general aspects and a synthesis of the results recently published in the literature on the structure and properties of investigated nanostructures. The main theoretical notions that allow the modeling of the behavior of semiconductor quantum systems are presented: the theory of effective mass, the theory of optical absorption, numerical methods for solving the Schrödinger equation for zero-dimensional structures under the action of external perturbations. The last part of the chapter contains a study of literature related to electro-optical phenomena in nanostructures, focusing on the phenomenon of electromagnetically induced transparency and the description of the behavior of quantum rings in GaAs / AlGaAs and self-assembled quantum points in InAs / GaAs in electric fields and magnetic fields.

2.7. Electro-optical phenomena in nanostructures-literature study

In recent years, quantum coherence and interference phenomena, such as coherent electron population control [55], terahertz emission [56] and electromagnetically induced transparency (EIT) [57] have attracted a great deal of interest both in the field of practical applications and related to theoretical research.

2.7.1. Electromagnetically Induced Transparency (EIT)

EIT is one of the most interesting effects of quantum optics, as it allows a coherent control of the optical properties of materials. In this effect, an opaque environment with three levels - atoms or nanostructures - subjected to a pair of laser, sample and control fields, may have low absorption windows (even zero) and a slowing down of the group speed of the laser sample [61]. The EIT phenomenon usually involves a three-tier system, with two dipole transitions allowed and a third forbidden. In general, depending on the transitions allowed or prohibited, the three-tier structure in which the EIT appears can be of the lambda scale (Λ), L (L- "ladder") or V scale (Figure 2.14.)

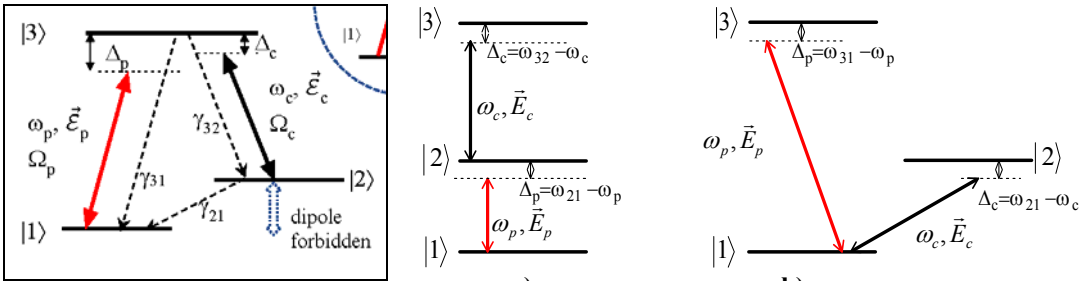

Figura 2.14 *Three-level system for the emergence of the EIT: a) type Λ configuration; b) L-type configuration, c) V-type configuration [62]*

QWs and QDs are excellent candidates for EIT investigation because they have discrete energy levels (like atoms) and in addition have the advantage of high values for nonlinear optical coefficients and dipole moments associated with intersband transitions. In these structures the energy levels and symmetry of the wave functions and, consequently, the transition frequency range and the absorption profile, can be conveniently modified in a wide range, which makes these structures interesting for practical applications. Consequently, theoretical and experimental studies on EIT in semiconductor nanostructures have been of constant interest in recent years.

The application of external fields offers the possibility of a convenient and efficient control of the characteristic sizes of the EIT (position and width of the transparency window, group speed).

Selective bibliography

[61] K.J. Boller, A. Imamolu, S. Harris, *"Observation of electromagnetically induced transparency"*, Phys. Rev. Lett. 66 (1991) 2593–2596.

[62] M.D. Lukin, A. Imamoglu, "*Controlling photons using electromagnetically induced transparency"*,Nature 413, 273 (2001)

Chapter 3

Effects of electric, magnetic and intense laser fields on the electromagnetically induced transparency in a semi-parabolic quantum well

3.1. Introduction

In the present chapter we investigate the electromagnetically induced transparency in a GaAs/Al0.3Ga0.7As semi-parabolic quantum well subjected to external electric, magnetic and non-resonant intense laser fields.

3.2. Theory

3.2.1. Semi-parabolic QW under electric , magnetic and non-resonant intense laser fields.

We consider a GaAs semi-parabolic QW grown along the *z*-direction, embedded between Al0.3Ga0.7As barriers of height V_0 (in the regions $z \le 0$ and $z \ge L$). The heterostructure is submitted to the joint action of electric and/or magnetic fields and an intense laser radiation. According to the effective mass theory, in the absence of the laser field, the Hamiltonian for the confined electron in the structure can be written as:

$$H = \frac{1}{2m^*}\left(\vec{p} + e\vec{A}\right)^2 + V(z) + eFz\,. \tag{3.1}$$

The first term of the Hamiltonian is the kinetic term of the electron under the influence of the magnetic field $\vec{B}$, m^* is the electron effective mass, *e* is the elementary charge, $\vec{p}$ is the electron momentum operator and *F* is the amplitude of the electric field oriented along the growth direction. *V (z)* is the semi-parabolic potential:

$$V(z) = \begin{cases} V_0 & z \le 0 \cup z \ge L \\ V_0 z^2 / L^2 & 0 < z < L \end{cases} \tag{3.2}$$

Taking the magnetic field parallel with the *x* direction, $\vec{B} = B\hat{x}$ ˆ , and using the nonsymmetric gauge $\vec{A} = -Bz\hat{y}$, the Hamiltonian in the z direction reduces to:

$$H = -\frac{\hbar^2}{2m^*}\frac{\partial^2}{\partial z^2} + V(z) + \frac{e^2B^2z^2}{2m^*} + eFz. \tag{3.3}$$

In order to consider the effects of a non-resonant laser field (NLF), represented by a monochromatic plane wave which is linearly polarized along z-axis, we use the Floquet method. In the high-frequency limit [26-28] the electron "sees" a laser-dressed confinement potential,

$$\widetilde{V}_{eff}(z, \alpha_0) = \frac{\omega_L}{2\pi}\int_0^{2\pi/\omega_L} V_{eff}\left(z + \alpha(t)\right)dt \tag{3.4}$$

where

$$V_{eff}(z) = V(z) + \frac{e^2B^2z^2}{2m^*}. \tag{3.5}$$

$\alpha(t) = \alpha_0 \sin(\omega_L t)$ describes the motion of the electron in the laser field and $\alpha_0 = \frac{eA_{0L}}{m^*\omega_L}$ is the laser-dressing parameter [26]. Here ω_L and A_{0L} is the angular frequency and the vector potential amplitude of NLF. The dressed potential has the analytical expression [29]:

$$\widetilde{V}_{eff}(z,\alpha_0)=\begin{cases} V_0+\dfrac{e^2B^2}{2m^*}\left(z^2+\alpha_0^2/2\right) & z\le-\alpha_0\cup z\ge L+\alpha_0 \\ \left(\dfrac{V_0}{L^2}+\dfrac{e^2B^2}{2m^*}\right)\left(z^2+\alpha_0^2/2\right)+\dfrac{V_0}{\pi}\arccos\left(\dfrac{z}{\alpha_0}\right)\left(1-\left(z^2+\alpha_0^2/2\right)/L^2\right)+\dfrac{3V_0z}{2\pi L^2}\sqrt{\alpha_0^2-z^2} & -\alpha_0<z\le\alpha_0 \\ \left(\dfrac{V_0}{L^2}+\dfrac{e^2B^2}{2m^*}\right)\left(z^2+\alpha_0^2/2\right) & \alpha_0<z\le L-\alpha_0 \\ \left(\dfrac{V_0}{L^2}+\dfrac{e^2B^2}{2m^*}\right)\left(z^2+\alpha_0^2/2\right)+\dfrac{V_0}{\pi}\arccos\left(\dfrac{L-z}{\alpha_0}\right)\left(1-\left(z^2+\alpha_0^2/2\right)/L^2\right) & \\ -\dfrac{V_0}{\pi L^2}\left(\dfrac{L+3z}{2}\right)\sqrt{\alpha_0^2-(L-z)^2} & L-\alpha_0<z<L+\alpha_0 \end{cases} \tag{3.6}$$

3.2.2 EIT in a three-level system

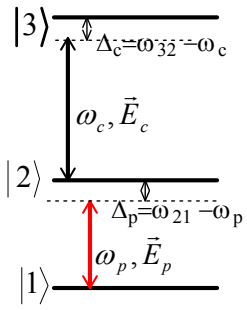

Figure 2.1. *Three energy levels in Ξ-configuration for EIT occurrence*

The interaction Hamiltonian is:

$$H_{\text{int}}(t)=-e\vec{\mu}\cdot\vec{E}\,. \tag{3.8}$$

with $\vec{\mu}$ the electric dipole moment operator and $\vec{E}$ the electric field amplitude of the applied laser pulses: $\vec{E}(\vec{r},t)=\dfrac{\vec{E}_p}{2}\left[\exp(i\omega_p t)+\exp(-i\omega_p t)\right]+\dfrac{\vec{E}_c}{2}\left[\exp(i\omega_c t)+\exp(-i\omega_c t)\right]$. (3.9)

In the rotating-wave approximation [30], we can represent the Hamiltonian of the threelevel Ξ-system interacting with the applied laser pulses as:

$$H=-\hbar\begin{bmatrix} 0 & \Omega_p & 0 \\ \Omega_p & -\Delta_p & \Omega_c \\ 0 & \Omega_c & -(\Delta_p+\Delta_c) \end{bmatrix}. \tag{3.10}$$

where Ωp and Ωc are half of the Rabi frequencies [30] and are defined as:

$$\Omega_p=\frac{\Omega_p^R}{2}=\frac{e\mu_{12}E_p}{2\hbar},\ \Omega_c=\frac{\Omega_c^R}{2}=\frac{e\mu_{23}E_c}{2\hbar}\ . \tag{3.11}$$

where μ_{21} and μ_{23} are the dipole moment matrix elements associated with the transition driven by the probe laser and the control laser,respectively.

The susceptibility of the three-level system, related to the probe field, is [1, 24]:

$$\chi = \frac{Ne^2\mu_{12}^2}{\varepsilon_0\hbar}\frac{-\delta + i\gamma_{31}}{\Omega_c^2 + (\gamma_{21} + i\Delta_p)(\gamma_{31} + i\delta)}. \tag{3.12}$$

where N is the density of the 3-level system and $\delta = \Delta p + \Delta c$. The real and imaginary parts of the susceptibility are:

$$\mathrm{Im}(\chi) = \frac{Ne^2\mu_{12}^2}{\varepsilon_0\hbar}\frac{\gamma_{21}(\gamma_{31}^2 + \delta^2) + \gamma_{31}\Omega_c^2}{(\Omega_c^2 + \gamma_{21}\gamma_{31} - \Delta_p\delta)^2 + (\Delta_p\gamma_{31} + \delta\gamma_{21})^2} \tag{3.13}$$

$$\mathrm{Re}(\chi) = \frac{Ne^2\mu_{12}^2}{\varepsilon_0\hbar}\frac{\delta(\Delta_p\delta - \Omega_c^2) + \Delta_p\gamma_{31}^2}{(\Omega_c^2 + \gamma_{21}\gamma_{31} - \Delta_p\delta)^2 + (\Delta_p\gamma_{31} + \delta\gamma_{21})^2}. \tag{3.14}$$

The probe laser induces the complex susceptibility that gives rise to a complex refraction index [24]:

$$(n_T(\omega) + i\kappa(\omega))^2 = n_r^2 + \chi(\omega) \tag{3.15}$$

where n_r is the static refractive index of the material and the real and imaginary parts read as:

$$n_T = \sqrt{\frac{n_r^2 + \mathrm{Re}(\chi) + \sqrt{(n_r^2 + \mathrm{Re}(\chi))^2 + \mathrm{Im}(\chi)^2}}{2}}, \qquad \kappa = \frac{\mathrm{Im}(\chi)}{2n_T}. \tag{3.16}$$

The absorption coefficient is related to the imaginary part of the susceptibility [30]:

$$\alpha(\omega) = \frac{2\omega\kappa}{c} = \frac{\omega\,\mathrm{Im}(\chi)}{cn_T} = \frac{\omega Ne^2\mu_{12}^2}{\varepsilon_0\hbar cn_T}\frac{\gamma_{21}(\gamma_{31}^2 + \delta^2) + \gamma_{31}\Omega_c^2}{(\Omega_c^2 + \gamma_{21}\gamma_{31} - \Delta_p\delta)^2 + (\Delta_p\gamma_{31} + \delta\gamma_{21})^2} \tag{3.17}$$

3.3 Results and discussion

The parameters used in our calculations are:
$V_0 = 228\,\mathrm{meV}$, L=25nm [29], $m^* = 0.067m_0$ [29] (where m_0 is the mass of a free electron), $N = 3\times10^{22}\ m^{-3}$, $n_r = 3.55$ [29], $\gamma_{31} = \gamma_{21} = 5\times10^{11}$ Hz [24].

3.3.1 Electronic properties

In Figure 3.2 a we represented the dressed potential of the semi-parabolic quantum well in the presence of the electric, magnetic and intense laser fields. We observe that for a positive oriented electric field the effective width of the QW is decreased and the right and left barrier are increased/decreased. The applied magnetic field determines a stronger decrement of the well width than the electric field and an increment of the left and right barriers that take now a parabolic form. The effect of the non-resonant laser is to increase the width of the upper part of the dressed potential and the minimum value of the potential, while the width of the bottom part decreases.

The displacement of the potential well toward higher values induced by the NLF leads to the increment of all levels of energy but also the levels get closer. Therefore the transitions energies are reduced with NLF strengthening. Thus the effect of the electric and magnetic fields is to increase the transition energies for low values of the NLF parameter. At larger values of this parameter the enlargement of the well induced by the NLF compensates the narrowing produced by the electric or magnetic fields and the energy is decreased.

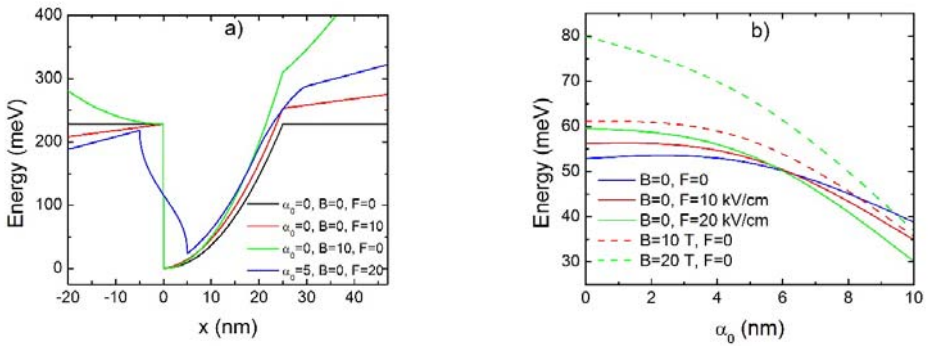

Figura 3.2 *a) The potential of the semi-parabolic QW and b) the transition energy E21 as function of the laser parameter α0 for different values of the external fields*

The transition moments are represented in Figure 3.3 function of the laser parameter for different values of the electric and magnetic fields.

In Figure 3.3 a we observe that the moments for 1→ 2 and 2 →3 transitions increase with the NLF strengthening. The electric and magnetic fields clearly influence their values, the magnetic field having a stronger influence. The moments for the 1→3 transition are very low in comparison with μ_{12}, μ_{23} and can be made practically zero with the proper choice of the external fields as can be seen in Figure 3.3 b.

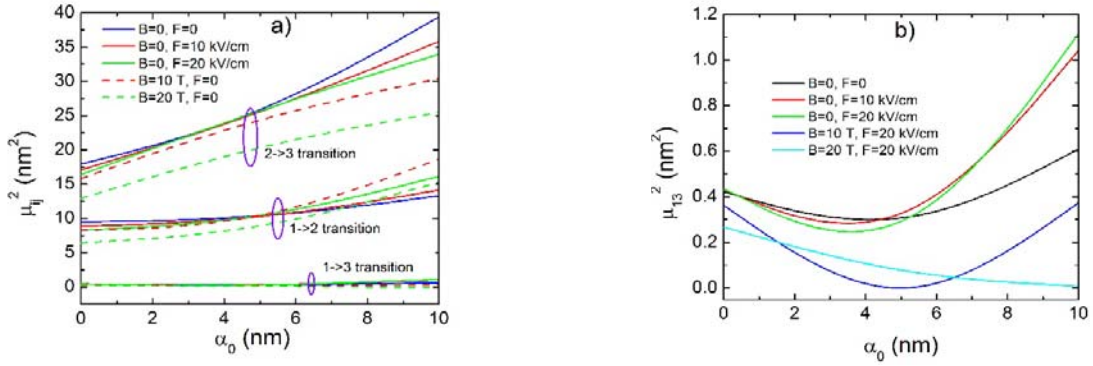

Figure 3.3 *a) The transition moments and b)* μ_{13}^2 *as function of the laser parameter* α_0 *for different values of the external field*

3.2 Optical properties

We represented the absorption coefficient (AC) and the refraction index (RI) as a function of the probe laser frequency ω p in Figs. 4-7 for different values of the external fields.

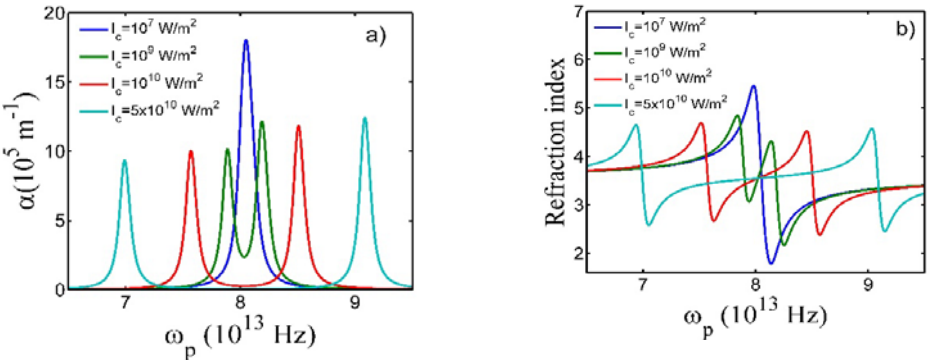

Figura 3.4. *a) The absorption and b) the refraction index as function of the probe frequency at four values of the control laser intensity.*

As can be seen in Figure 3.4 a, at low intensity of the control laser (I_c=10^7 W/m^2 or lower) the absorption has a Lorentzian profile with maximum at $\omega_p = \omega_{21}$ if $\Delta_c = 0$, $\delta = \Delta p$, so the transparency cannot be induced. The refraction index has a negative slope (anomalous dispersion) in the narrow region centered on $\omega_p = \omega_{21}$ (see Fig. 3.4b). At larger intensities, the absorption presents two unequal maxima and a minimum at $\omega_p = \omega_{21}$ if the following condition is fulfilled [20, 24]:

$$\Omega_c > \frac{\gamma_{31}\sqrt{\gamma_{31}}}{\sqrt{\gamma_{21}+2\gamma_{31}}} \tag{3.18}$$

The control laser intensity is related to Ωc by $I_c = \frac{\varepsilon_0 c n_r E_c^2}{2} = \frac{2\hbar^2 \varepsilon_0 c n_r \Omega_c^2}{e^2 \mu_{23}^2}$.

However, we observe that even at I_c=5x10^{10} W/m^2 the transparency is still not perfect, the absorption having a residual value. At I_c=5x10^{10} W/m^2 we can say that the transparency is quite good, because in this case, the condition of EIT occurrence $\alpha_{min} \le 10^{-3}\alpha_{max}$ is respected [18].

In Figure 3.5 we depicted the AC and RI for three values of the NLF parameter α_0 in the absence of the electric and magnetic fields.

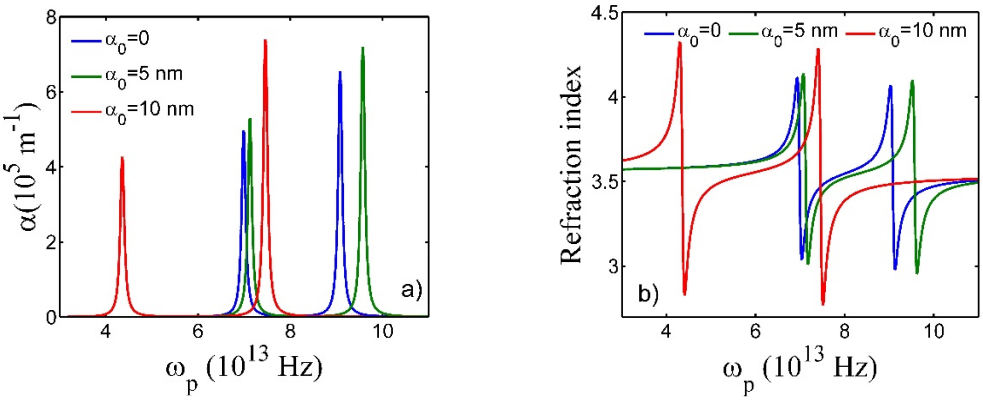

Figure 3.5. *a) The absorption and b) the refraction index as function of the probe frequency for three values of the NLF parameter, at B=0 and F=0.*

Some effects are noticeable in Figure 3.5 at the augment of α_0: i) the AC and RI peaks increase due to the μ_{12} increment; ii) the TW value increases according to the μ_{23} raise that induces the augment of Ω_c; iii) the TW goes first to higher probe frequencies at α_0. Note that α_{min} decreases at the increment of Ω_c, thus the condition $\alpha_{min} \le 10^{-3}\alpha_{max}$ is always respected.

In Figure 3.6 we illustrated AC and RI at different values of the electric field in the presence of ILF, but in the absence of the magnetic field.

We observe that the width of the transparency windows is almost constant because μ_{23} remains quasi-constant for this particular choice of external fields, but is blue-shifted at the electric field strengthening due to the raise of the transitions energy E_{21}.

In order to see the influence of the magnetic field on the EIT characteristics we represented in Figure 3.7 the AC and RI at different values of the magnetic field for the NLF parameter α_0 =5 nm.

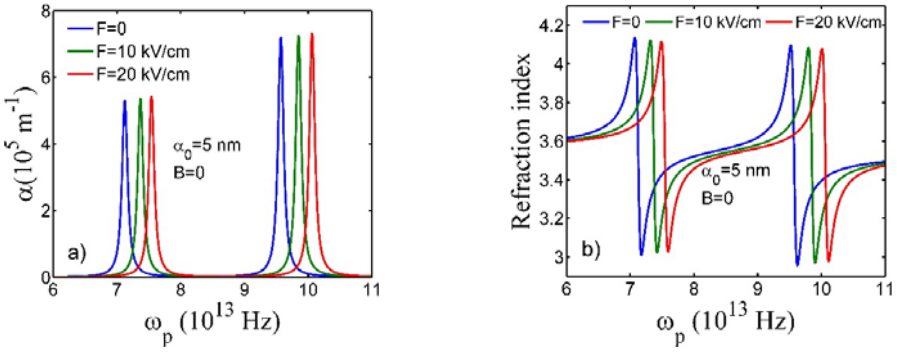

Figure 3.6 *a)The absorption and b) the refraction index as function of the probe frequency for three values of the electric field for α_0=5 nm and B=0.*

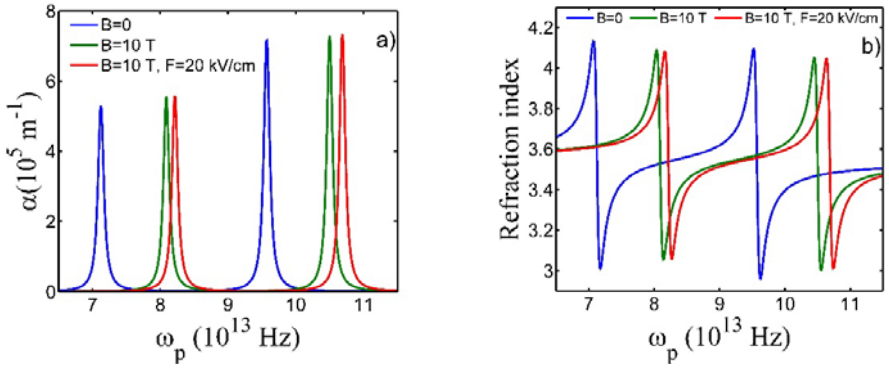

Figure 3.7. *a) The absorption and b) the refraction index as function of the probe frequency for two values of the magnetic field and α_0=5 nm.*

Analyzing Figure 3.7, we notice that: (i) the electric field was absent for the blue and green curves but was set to F=20 kV/cm for the red curve because for this choice of parameters $\mu_{13} = 0.015\,\text{nm}$, favoring the EIT occurrence in the semi-parabolic well; (ii) the most interesting effect is the blueshift of the transparency windows caused by the E_{21} increment with B. (iii) the peaks magnitude and TW width are almost constant for F or B variation at α_0 =5 nm. The transparency window width will be strongly increased (decreased) by the augment (diminution) of the NLF intensity.

3.4. Conclusions

Our main findings are: i) the EIT occurs in the system in all cases but it is advantaged by a proper choice of the external fields; ii) the increase of the non-resonant laser intensity strongly enlarges the transparency window width; iii) the transparency window for absorption of the probe laser is blue-shifted by the augment of the electric or magnetic field strength. iiii) The system allows a rather large transparency window at rather low.

3.5 Selective bibliography

[24] D. Bejan, "*Electromagnetically induced transparency in double quantum dot under intense laser and magnetic fields*: *from Λ to Ξ Configuration*", Eur. Phys. J. B, 90 (2017) 54.
[25] D. Bejan, "*Exciton effects on the nonlinear optical properties of semiparabolic quantum dot under electric field"*, Eur. Phys. J. Plus, 132 (2017)102.
[26] M. Gavrilă, J.Z. Kaminski, Free-Free *Transitions in Intense High-Frequency Laser Fields*, Phys. Rev. Lett. **52** (1984) 613.
[29] F. Ungan, J.C. Martínez-Orozco, R.L. Restrepo, M.E. Mora-Ramos, E. Kasapoglu, C.A. Duque, "*Nonlinear optical rectification and second-harmonic generation in a semi-parabolic quantum well under intense laser field: Effects of electric and magnetic fields*", Superlatt. Microstruct. **81** (2015) 26-33.

Chapter 4

Magnetic field control of absorption coefficient and group index in an impurity doped quantum disc

The results presented in this chapter were published in "The European Physical Journal B" (2017),) DOI: 10.1140 / epjb / e2017-80138-0

4.1 Introduction

The electronic properties and optical characteristics - absorption coefficient, refractive index and group index - in an impurity doped pseudoharmonic quantum disc subjected to an applied magnetic field are investigated.

This work is devoted to a theoretical study of the optical properties in a doped GaAs PHQD related to the occurrence of the electromagnetically induced transparency (EIT) phenomenon.

4.2. Theory

We consider an electron in the conduction band in a QR with inner, outer radius (R_1 (R_2)) and height L_z, under the simultaneous action of the Coulomb attraction due to an ionized donor and a magnetic field parallel to the z axis. For an almost plane QR, for which the condition is met, we can use the adiabatic approximation and decouple the motion along the z axis from that in the xy plane. In this case, the main characteristics of the spectrum are essentially determined by the confinement in the xy plane. The confinement potential, which combines the parabolic and inverse quadratic potential functions, is represented in Figure 4.1 in the presence of a donor impurity for different values of the magnetic field.

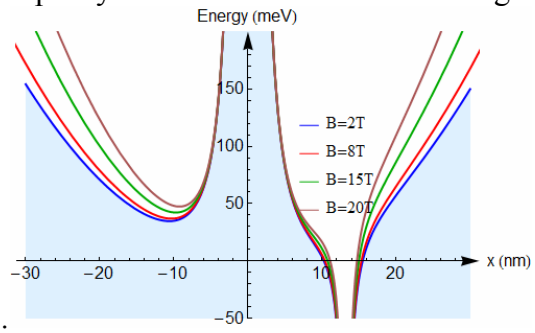

Figure 4.1 *The confinement potential energy along x-direction (including the Coulomb interaction) in a GaAs PHQD for different magnetic field strengths. Results are for λ = 2, ω_0 = 20 THz and the impurity placed in* $x_0 = \sqrt{\hbar\lambda / m^*\omega_0}$.

Using polar coordinates $(r,\varphi)$and the Coulomb gauge $\vec{A} = (0, Br/2)$, the Hamiltonian H takes the form [8,42]:

$$H_0 = -\frac{\hbar^2}{2m^*}\left(\frac{\partial^2}{\partial r^2}+\frac{1}{r}\frac{\partial}{\partial r}+\frac{1}{r^2}\frac{\partial^2}{\partial \varphi^2}\right)+\frac{\hbar^2}{2m^*}\frac{\lambda^2}{r^2}+\frac{1}{2}m^*\left(\omega_0^2+\left(\frac{eB}{2m^*}\right)^2\right)r^2+\frac{\omega_c}{2}L_z \quad (4.4),$$

where $\omega_c = \frac{eB}{m^*}$ the cyclotron frequency and Lz is the orbital angular momentum operator along the z-direction. In the absence of the impurity, eigenstates of the corresponding Schrodinger equation can be exactly described via analytical expressions [8, 42]:

$$\psi^0_{nm}(r,\varphi) = N_{nm}\frac{\xi_{nm}(r)}{\sqrt{r}}e^{im\varphi}, \tag{4.5}$$

where N_{nm} is normalization constant and $m = 0, \pm1, \pm2, \ldots$ is the magnetic quantum number .

The radial function $\xi_{nm}(r)$ is given by:

$$\xi_{nm}(r) = r^{t_m}e^{-r^2/2\eta^2}L_n^{(t_m+1/2)}\left(r^2/\eta^2\right). \tag{4.6}$$

where $\eta = \sqrt{\hbar/m^*\Omega}$ with $\Omega = \sqrt{\omega_0^2 + \left(\frac{eB}{2m^*}\right)^2} = \sqrt{\omega_0^2 + \omega_c^2/2}$, $t_m = 1/2 + \sqrt{\lambda^2 + m^2}$ and $L_n^{(t_m+1/2)}$ is the generalized Laguerre polynomial of order n.

The eigenvalues of Hamiltonian H_0 have the following expression [8, 42]:

$$E^0_{nm} = \left(2n + 1 + \sqrt{\lambda^2 + m^2}\right)\hbar\Omega + m\hbar\omega_c \tag{4.7}$$

The eigenfunctions of the equation:

$$\left(H_0 - \frac{e^2}{4\pi\varepsilon_0\varepsilon_r|\vec{r} - \vec{r}_i|}\right)\Psi(\vec{r}) = E\Psi(\vec{r}) \tag{4.8}$$

can be expanded as a linear combination of the eigenfunctions of Hamiltonian H_0:

$$\Psi(r,\varphi) = \sum_{n,m} C_{nm}\psi_{nm}(r,\varphi), \tag{4.9}$$

At low magnetic fields there are some particular values of B for which the highest energy state $|3\rangle$ has a nonzero coupling dipole moment to both $|1\rangle$ and $|2\rangle$ states, whereas the transition $1 \rightarrow 2$ is a dipole-forbidden one. These characteristics define a three-level system in a Λ-type configuration, shown in Figure 4.2 a.

For high magnetic fields (B > 10 T), $1 \rightarrow 2$ and $2 \rightarrow 3$ are dipole-allowed transitions while $1 \rightarrow 3$ is a dipole-forbidden one, thus defining an L-type configuration (shown in Figure.4. 2b).

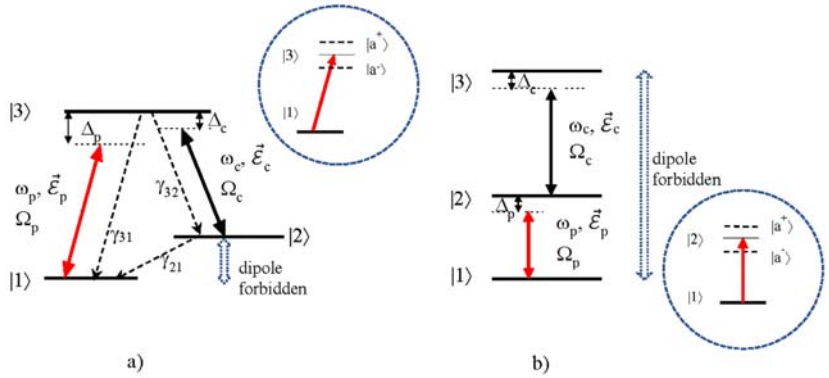

Figure 4.2. *Three-level system for EIT occurrence: (a)* ***A****-type configuration and (b)* ***L****-type configuration. Closed in dashed circles are the corresponding dressed states*

The susceptibility of the three-level system related to the probe field is given through the matrix element $\rho_{p1} = \rho^*_{1p}$ [46]:

$$\chi = \frac{2N\rho_{p1}\mu_{p1}}{\varepsilon_0 E_p}, \tag{4.15}$$

where N is the electron density of the system. Consequently, the susceptibility of the three-level system in the A-configuration is given by [50]:

$$\chi^{\Lambda} = \frac{N\mu_{31}^2}{\varepsilon_0\hbar}\frac{-(\Delta_p-\Delta_c)+i\gamma_{21}}{\Omega_c^2+(\gamma_{31}+i\Delta_p)(\gamma_{21}+i(\Delta_p-\Delta_c))}, \tag{4.16}$$

where γ_{31} and γ_{21} are the spontaneous decay rates for the transition driven by the probe field and the dipole forbidden transition, respectively.

For the **L**-configuration, the susceptibility can be written as [41]:

$$\chi^{L} = \frac{N\mu_{21}^2}{\varepsilon_0\hbar}\frac{-(\Delta_p+\Delta_c)+i\gamma_{31}}{\Omega_c^2+(\gamma_{21}+i\Delta_p)(\gamma_{31}+i(\Delta_p+\Delta_c))}. \tag{4.17}$$

For the probe radiation, the refractive index and the absorption coefficient are obtained from *x* [49] as:

$$n_T = \sqrt{\frac{n_r^2+\mathrm{Re}(\chi)+\sqrt{(n_r^2+\mathrm{Re}(\chi))^2+\mathrm{Im}(\chi)^2}}{2}} \tag{4.21}$$

and

$$\alpha(\omega_p) = \frac{\omega_p}{c\,n_r}\mathrm{Im}\chi(\omega_p) \tag{4.22}$$

respectively, where n_r is the static refractive index of the material. The group velocity v_g of the probe light pulse is found [51] using the definition:

$$v_g = \frac{c}{n_T(\omega_p)+\omega_p\frac{\mathrm{d}\,n_T}{\mathrm{d}\,\omega_p}}, \tag{4.23}$$

and the group index *ng* is given by:

$$n_g = \frac{c}{v_g} = n_T(\omega)+\omega\frac{\mathrm{d}\,n_T}{\mathrm{d}\,\omega}. \tag{4.24}$$

4.3 Results and discussion

The physical parameters used for the numerical computation for a typical GaAs PHQD [41] are $N = 3\cdot10^{21}$, $\gamma_{21} = \gamma_{31} = 3\cdot10^{10}$ Hz and the relative dielectric constant = 12.85. The values for the potential parameters were taken as $\lambda^2 = 4$ and $\omega_0 = 20$ THz.

Figure 4.5 presents the optical characteristics versus the probe frequency for different Qc values when B = 2 T (**Λ** type configuration) and zero control field detuning.

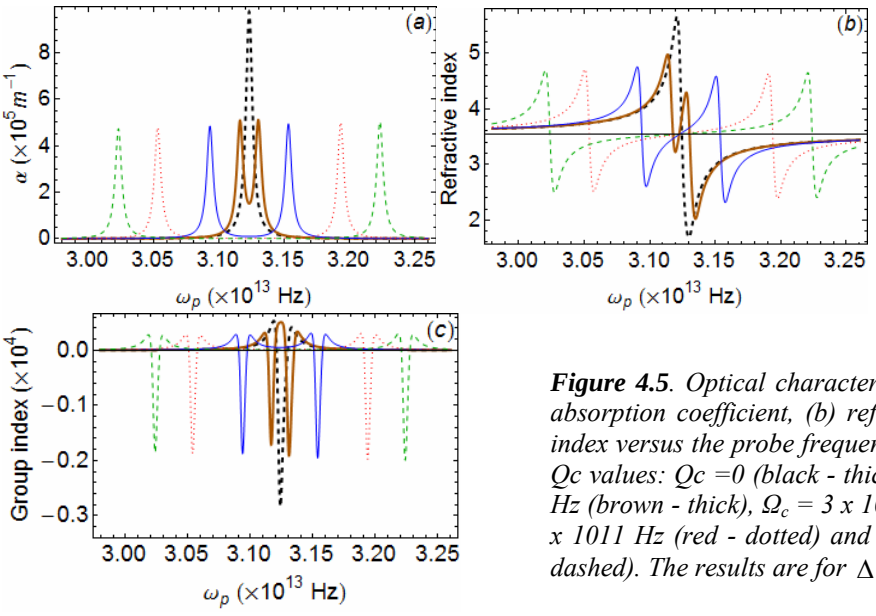

***Figure 4.5**. Optical characteristics for A-type system: (a) absorption coefficient, (b) refractive index and (c) group index versus the probe frequency for B = 2 T and different Qc values: Qc =0 (black - thick dashed), Ω_c = 0.7 x 1011 Hz (brown - thick), Ω_c = 3 x 1011 Hz (blue - thin), Ω_c c= 7 x 1011 Hz (red - dotted) and Ω_c = 1012 Hz (green - thin dashed). The results are for Δ_c = 0.*

Figure 4.6 shows the same physical parameters as in Figure 4.5 but for B = 20 T (L-configuration).

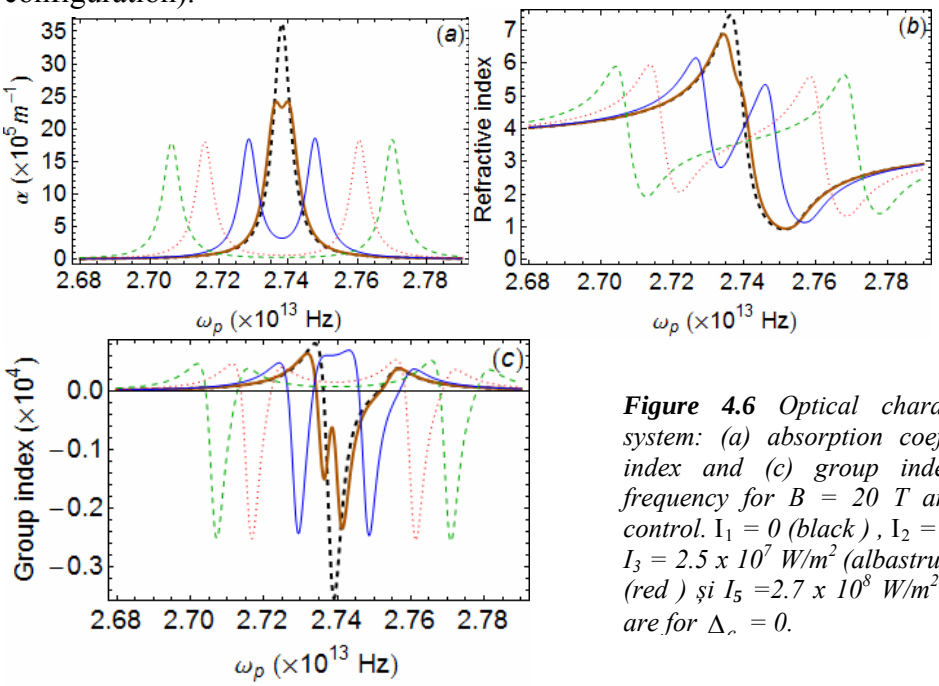

Figure 4.6 *Optical characteristics for L-type system: (a) absorption coefficient, (b) refractive index and (c) group index versus the probe frequency for B = 20 T and different values of control.* I_1 *= 0 (black) ,* I_2 *= 1.3 x* 10^6 *W/m*^{2} *(thin),* I_3 *= 2.5 x* 10^7 *W/m*^{2} *(albastru),* I_4 *= 1.3 x* 10^8 *W/m*^{2} *(red) şi* I_5 *=2.7 x* 10^8 *W/m*^{2} *(green). The results are for* $\Delta_c = 0$.

However, by analyzing Figures 4.5 and 4.6 some particular characteristics can be emphasized: (i) the peak values of AC, mainly determined by the product $\omega_{p1}\cdot\mu_{p1}^2$, are obviously increased for the *L*-configuration despite of the slighter values of E_{12} transition energy. This is because, accordingly to the comments in Figure 4.3, $\mu_{21}(B=20T)>\mu_{31}(B=2T)$;(ii) for L-type system, AC curves are lesser sensitive to the control laser intensity. For example, when *Ic* = 1.3 x 10^6 W/m^2 (brown curves in Figure 4.6) the absorption does not fall significantly and the dispersion keeps the anomalous regime behavior. Even for *Ic* = 2.5 x 10^7 W/m^2 the transparency is no longer perfect (see blue curve in Figure 4.6.a, which shows a significant residual value, absent in the corresponding curve from Figure 4.5. a).

Figures 4.7 and 4.8 show the effect of the magnetic field on the optical properties for both studied configurations when the intensity of the control laser has the value *Ic* = 10^9 W/m^2

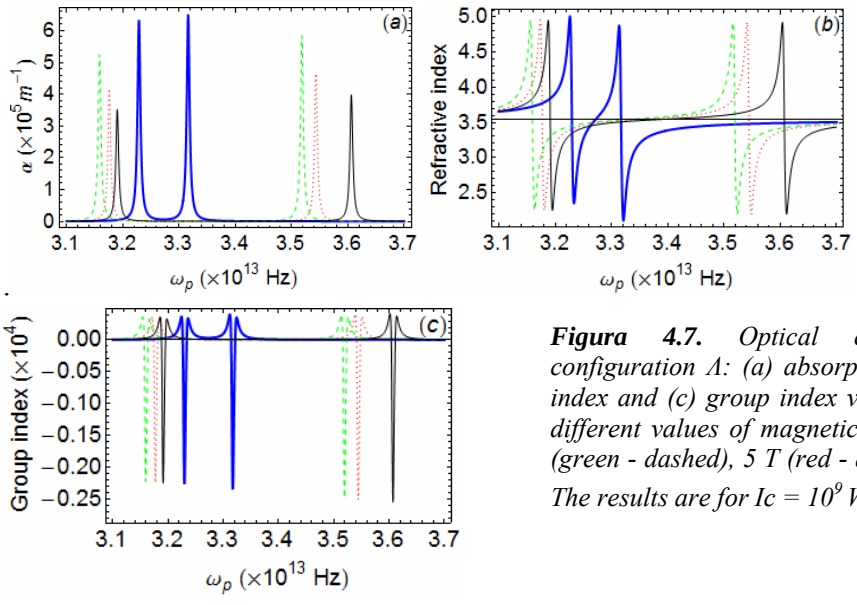

Figura 4.7. *Optical characteristics for A-type configuration Λ: (a) absorption coefficient, (b) refractive index and (c) group index versus the probe frequency for different values of magnetic field: 3 T (blue - thick), 4 T (green - dashed), 5 T (red - dotted), and 6 T (black - thin). The results are for Ic =* 10^9 *W/m*^{2} *and* $\Delta_c = 0$

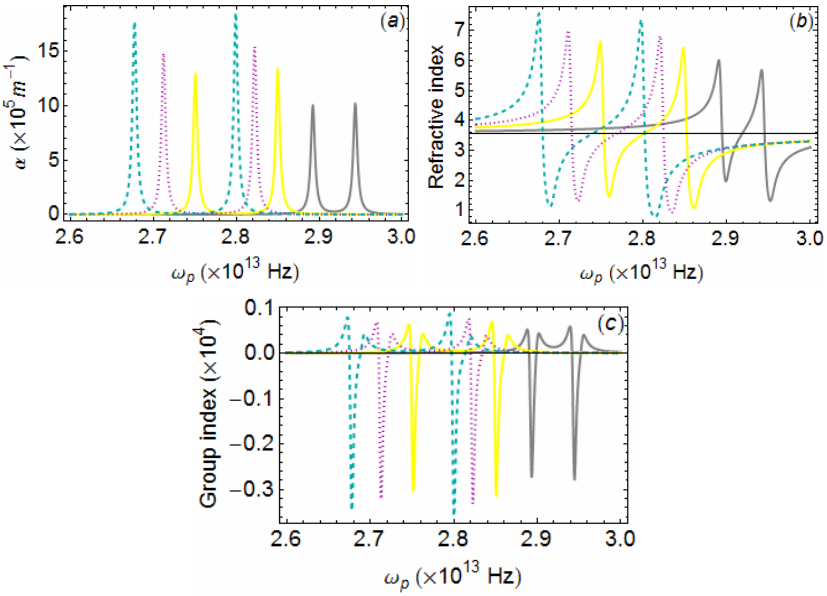

Figura 4.8. *Optical characteristics for A-type configuration* ***L****: (a) coeficientul de absorbție(a) absorption coefficient, (b) refractive index and (c) group index versus the probe frequency for different values of magnetic field: 17 T (gri), 18 T (yellow),19 T (magenta) și 20 T (thin). Rezultatele sunt pentru* $I_c = 10^9\ W/m^2$ *și* $\Delta_c = 0$.

Figures 4.7 and 4.8 show that by increasing the magnetic field, TW slightly moves toward higher values of the laser probe frequency in the case of A-configuration, while it is red- shifted for the L-type structure. Besides, in latter case the peaks of RI and GI are more sensitive to the field variation and show a significant growing of the positive maximum with B. Moreover, for high magnetic fields in the anomalous dispersion region a fast light propagation (as well as high-speed backward propagation) could be achieved (see cyan - dashed curve in Figure 4.8c).

The effect of the control field detuning on EIT for the PHQD system is depicted in Figures 4.9 and 4.10 for $I = 10^9$ W/m^2 and $\Delta c = 5\ \gamma_{21}$. For an easily understanding of the results, we plot the dependence of the optical characteristics on the probe field detuning, Δ_p

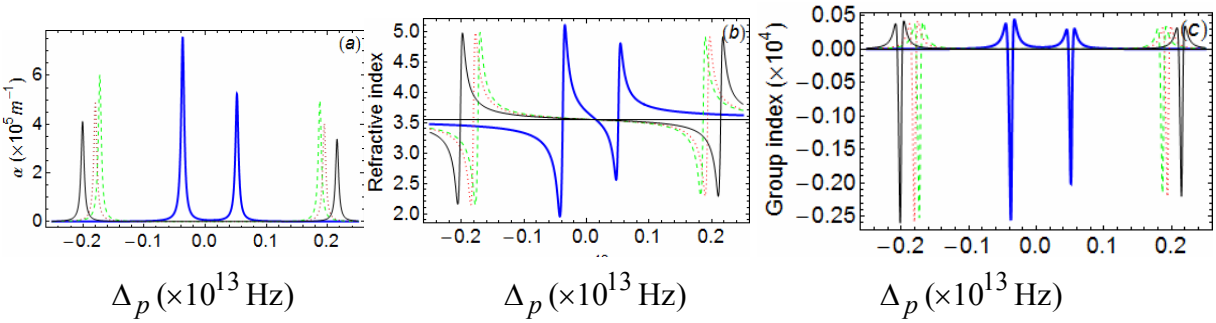

Figura 4.9. *Optical characteristics for Λ-type configuration: (a) absorption coefficient, (b) refractive index and (c) group index versus the probe detuning for different values of magnetic field: 3 T (blue – thick), 4 T (green – dashed), 5 T (red – dotted), and 6 T (black – thin).*
The results are for $I = 10^9\ W/m^2$ *and* $\Delta_c = 5\gamma_{21}$.

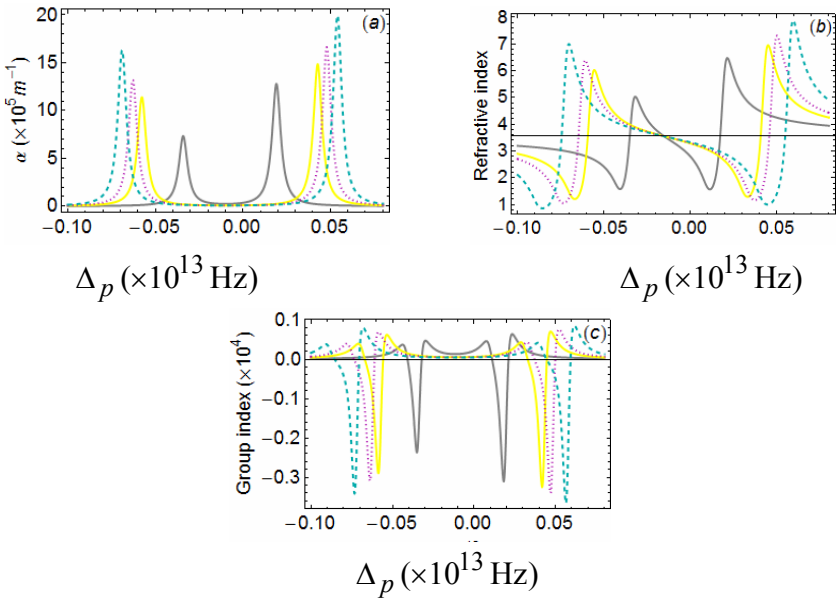

Figura 4.10 *Optical characteristics for L-type configuration: (a) absorption coefficient, (b) refractive index and (c) group index versus the probe detuning for different values of magnetic field: 17 T (gray – thick), 18 T (yellow – thin), 19 T (magenta – dotted), and 20 T (cyan – dashed).*
The results are for $I = 10^9$ *W/m*^{2} *and* $\Delta_c = 5\gamma_{21}$.

We underline some noticeable differences between the studied configurations: (i) TW is centered on a value Δp > 0 (Δp < 0) for the Λ- (L-) configuration, for which the two-photon resonance condition Δp − Δc =0 (Δp + Δc = 0) is accomplished; (ii) the transmission profile and the associated dispersion become highly asymmetrical; (iii) increased positive maxima of the group index and faster backward propagation in the high-(low-)frequency region of the probe field is obtained for the Λ-type (L-type) system.

4.4 Conclusions

In this study, we have investigated the electromagnetically induced transparency in a GaAs two-dimensional pseudo-harmonic quantum dot subjected to an external applied magnetic field. We demonstrated that the energy spectrum exhibits two possible configurations as a function of the magnetic field strength. Moreover, the positions and amplitudes of the absorption peaks and group index extrema exhibit significant dependences on the applied magnetic field and on the impurity position. The particular geometry of the system allows rather large transparency windows and reasonable values of the threshold control field amplitude associated with EIT mechanism.

4.5 Selective bibliography

[8] C.M. Duque, M.E. Mora-Ramos, C.A. Duque, "*Quantum disc plus inverse square potential. An analytical model for two□dimensional quantum rings: Study of nonlinear optical properties*", Ann. Phys. (Berlin) 524, 327 (2012)
[41]V. Pavlović, L. Stevanović, "Electromagnetically induced transparency in double quantum dot under intense laser and magnetic fields: from Λ to Ξ configuration", Superlatt. Microstruct. 92, 10 (2016)
[42] G. Liu, K. Guo, C. Wang, "*Linear and nonlinear intersubband optical absorption in a disk-shaped quantum dot with a parabolic potential plus an inverse squared potential in a static magnetic field*", Physica B 407, 2334 (2012)
[46] M. Fleischhauer, A. Imamoglu, J.P. Marangos, "*Electromagnetically induced transparency: Optics in coherent media*", Rev. Mod.Phys,77, 633 (2005)
[49] D. Bejan, Eur. J. Phys. B, https://doi.org/10.1140/epjb/e2017-70738-y.
[50] N. Liu, Y. Zhang, C. Kang, Z. Wang, B. Yu, "*Two-dimensional probe absorption in coupled quantum dots*", Physica E 81, 248 (2016)
[51] R.W. Boyd, *"Nonlinear Optics",* 3rd Ed. Academic Press, San Diego, (2008), Chap. 6.

Chapter 5

Stark shift and oscillator strenghts in a GaAs quantum ring with off-center donor impurity.

The study presented in this chapter was published in the ***U.P.B. Sci. Bull., Series A, Vol. 80, Iss. 1, 2018***

5.1 Introduction

In this chapter, we study the electric field effects on the Stark-shift of impurity ground state in a two-dimensional quantum ring represented by a pseudoharmonic potential. The energy spectra and wave functions are obtained within the effective mass approximation by using a finite element method [24].

5.2 Theory

In the framework of the effective mass approximation and choosing the electric field direction as x-axis, the single-particle Hamiltonians:

$$H = H_0 + eFx - \frac{e^2}{4\pi\varepsilon_0\varepsilon_r|\vec{r}-\vec{r}_i|} \tag{5.1}$$

where

$$H_0 = -\frac{\hbar^2}{2m^*}\Delta + V(\vec{r}) \tag{5.2}$$

$\vec{r} = (x, y)$ is the in-plane vector position for the electron, ε_0 the vacuum dielectric permittivity, ε_r the static dielectric constant of the ring material $\vec{r}_i = (x_i, y_i)$ is the impurity position inside the ring and Δ is the two-dimensional Laplacean operator. The confining potential, *V(r)*, combines the parabolic and inverse square potential functions:

$$V(r) = \frac{\hbar^2}{2m^*}\frac{\lambda^2}{r^2} + \frac{1}{2}m^*\omega_0^2 r^2 . \tag{5.3}$$

The dimensionless parameter, λ, characterizes the strength of the inverse square potential which describes the forbidden hollow region inside the ring [25, 26] and ω_0 is the confinement frequency of the parabolic potential.

The change in the electron distribution within the nanostructure induced by a static electric field is described by the so called static dipole polarizability. It is well known that the quantum-confined Stark effect leads to a shift of the ground state energy given by:

$$\Delta E(F) = E(F) - E(F=0) = -\vec{p}\cdot\vec{F} - \frac{1}{2}\beta F^2 . \tag{5.4}$$

This quadratic form follows from a second-order perturbation theory with p ρ the dipole moment and β the polarizability of the system [27]. For F along the x-direction β is given by [27- 29]:

$$\beta = -\frac{e}{F}\left[\langle x\rangle_F - \langle x\rangle_{F=0}\right] = -\frac{e}{F}\left[\langle\Psi_1(\bar{r})|x|\Psi_1(\bar{r})\rangle_{F\neq 0} - \langle\Psi_1(\bar{r})|x|\Psi_1(\bar{r})\rangle_{F=0}\right] \tag{5.5}$$

where $p = \beta F$.

The oscillator strength for a transition from level *i* to level *n* is obtained from standard formula as [30] :

$$f_{ni} = \frac{2m_0}{\hbar^2} \Delta E_{in} \left|\mu_{in}\right|^2 \tag{5.6}$$

where $\Delta E_{in} = E_n - E_i$ is the energy difference between the electron states and

$$\mu_{ij} = \left\langle \Psi_i(x,y) \middle| r \middle| \Psi_j(x,y) \right\rangle \tag{5.7}$$

is the transition matrix element in the dipolar approximation. In Eq. (5.7), *r* refers to *x* for a *x*-polarized (along the electric field direction) and *y* for a *y*-polarized incident light, respectively.

5.3. Results and discussion

In the following I describe some of the most suggestive graphs, as well as the observations corresponding to the chosen graphic sets. The adjustable parameters of the ring potential are chosen as $\lambda^2 = 4$ and $\omega_0 = 20$ THz, so that the carriers are confined between the inner radius R_1=2.7 nm and the outer radius R_2=62.8 nm, corresponding to Vo ≈ 300 meV, Lz =2 nm, Three positions of the hydrogenic donor within the structure are considered in our study: $(r_0,0)$, $(-r_0,0)$ și $(0,r_0)$.

The Stark shift dependence on the donor location is plotted in Figure 5.2 as a function of the electric field.

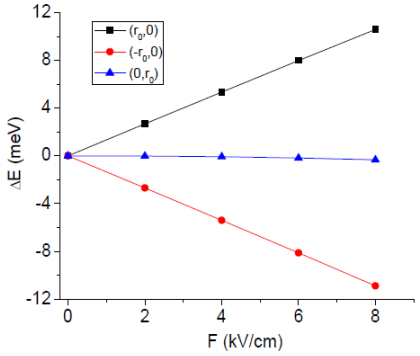

Figure 5.2 *Stark shift as a function of the electric field strength for off-center donors in a GaAs QR. The impurity is located at three different positions:* $(r_0,0)$, $(-r_0,0)$, *and* $(0,r_0)$, *respectively.*

For impurity placed along (opposite) field direction, the energy shift linearly increases (decreases) with the electric field. As expected, for a donor localized in $(0,r_0)$, when the charge distribution is less sensitive to the field influence, the Stark shift is not significantly changed by the electric field.

Figure 5.3 displays the variation of the polarizability and the dipole moment for a shallow donor in a QR versus the electric field for different values of the impurity position.

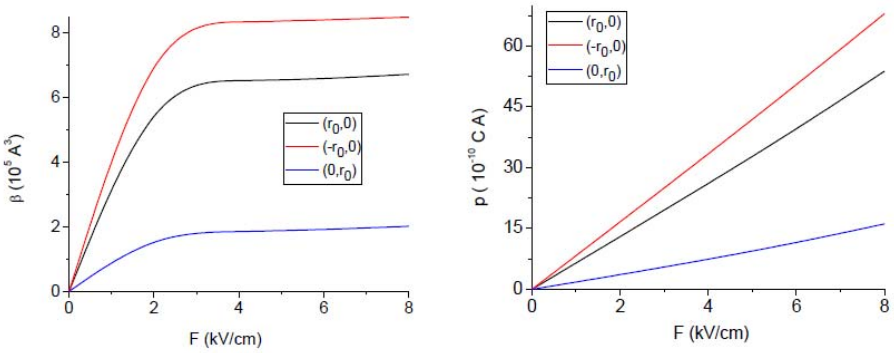

Figure 5.3. *The impurity polarizability (left) and dipole moment (right) as a function of the lateral electric-field amplitude F. Same impurity positions as in Fig. 5.2 are considered.*

One observes that the polarizability increases as the applied field is increased and tends to saturation for rather small values of the electric field. The saturation for these three impurity positions has different explanations: (i) for localization along the field direction (black curve) it is the results of the competition between the Coulomb attraction (which keeps the electron cloud around the donor center, in the right side of the ring) and electric field effect (which pushes the carriers in the opposite (-*x*) direction, (ii) when the impurity is placed at $(-r_0,0)$ (red curve), the behavior results from the strong confinement under combined effect of the Coulomb potential and the field-induced leakage of the electron wave function towards the left region, where the well bottom is shifted to lower energies. This increased confinement of the electron cloud leads to the poor impurity deformability under the electric field influence. (iii) for impurity placed along *y*-direction (blue curve) the polarizability is weaker because the effect of the field-related changes in the electron-impurity localization is small, as discussed before. All the curves in As expected, the impurity placed along or perpendicular to field direction (black and blue curves in Figure 5. 3(b)) becomes less sensitive to field variations due to a weaker quantum confinement.
Dependences of these quantities on the applied electric field is plotted in Figs. 5.4. and 5.5.

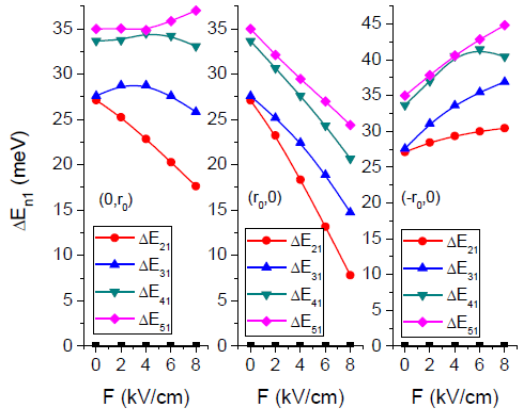

Figure 5.4. *Energy differences* ΔE_{n1} *versus applied electric field* $|\mu_{1n}|^2$ *for the same impurity positions as in Fig. 5.5.*

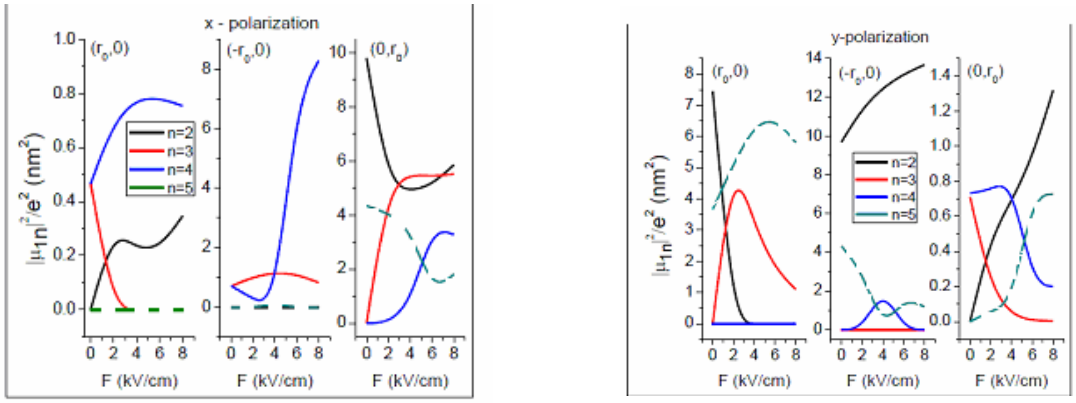

Figure 5.5. *The transition matrix element* $|\mu_{1n}|^2$ *versus the applied electric field. Two polarizations of the incident light and three impurity position in the QR are considered.*

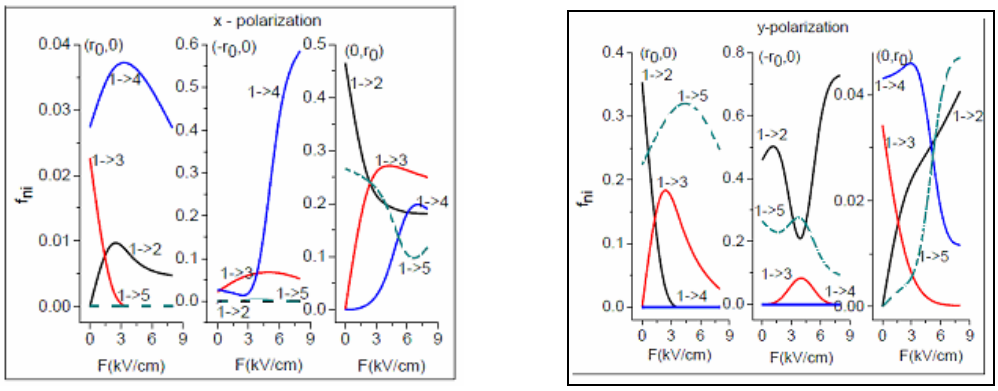

Figura 5.6. *Oscillator strength for the ground-to-lowest excited states transitions versus applied electric field for x- (left panel) and y- (right panel) polarization of the incident light. The same three impurity positions as in Fig. 5.2 are considered .*

By comparing the results in two panels we notice that:

- $|\mu_{in}|^2$ (which is very sensitive to the incident light polarization) is the dominant term in the OS behavior.
- when the impurity is placed in right side of the ring, the intensity of interlevel transitions induced by *y*-polarized light is at least one order of magnitude larger than those corresponding to a *x*-polarization.
- for the $(r_0,0)$ location, when OS has appreciable values for the *x*-polarization.
- for a donor placed on left side of the ring the interlevels transitions show a very different behavior (see middle figures in panels). We note that the transitions $1\rightarrow2$ and $1\rightarrow5$, dominant for the *y*-polarized light, becomes practically forbidden for a *x*-polarization.
- the oscillator strength of $1 \rightarrow 4$ interlevel transition (which vanishes for a y-polarized light) dramatically increases with *F* for the *x*-polarized incident radiation.

5.4. Conclusions

In this chapter, we have theoretical analyzed the effect of a lateral electric field on the Stark-shift, polarizability and oscillator strength associated to off-center donor impurities in a GaAs disc-shaped quantum ring. Using the finite difference method in the effective mass approximation, we found that in the range of the moderate field values the Stark-shift exhibits a linear dependence, and the impurity polarizability tends to saturation values. The behavior of the oscillator strength associated with impurity interlevel transitions shows a strong dependence both on the incident light polarization and on the impurity position within the Stark shift and oscillator strengths in a GaAs quantum ring with off-center donor impurity. Because of the close relationship between the intraband absorption and the corresponding oscillator strength, our results should provide useful guidance for the design of more efficient quantum-ring infrared photodetectors.

5.5. Selective bibliography

[24] R. D. Cook, D. S. Malkus, M. E. Plesha, "*Concepts and Applications of Finite Element Analysis*",3rd edition, John Wiley & Sons, New York, 1989.

[25] R. E. Acosta, A. L. Morales, C. M. Duque, M. E. Mora-Ramos, and C. A. Duque, "*Optical absorption and refractive index changes in a semiconductor quantum ring: Electric field and donor ipurity effects"*, Phys. Status Solidi B 253 (2016), pp. 744–754.

[26] G. Liu, K. Guo, C. Wang, "*Linear and nonlinear intersubband optical absorption in a diskshaped quantum dot with a parabolic potential plus an inverse squared potential in a static magnetic field*," Physica B 407, 2012, pp. 2334-39.

Chapter 6

Magnetic-field dependence of the impurity states in a dome-shaped quantum dot

The study presented in this chapter was published in ***"Chemical Physics", volume 493, pag. 32-41, (2017)***

6.1. Introduction

The present chapter attempts to fill this gap in the literature by a detailed investigation of the electronic probability density, energy levels, transition frequencies and diamagnetic susceptibility of hydrogenic donors in a dome-shaped InAs/GaAs QD coupled to its WL and subjected to a magnetic field.

6.2.Theory

In this study, a dome-shaped InAs/GaAs QD with radius R =7 nm grown on a 2 nm wetting layer is considered (see inset of Figure 7.1a). The *x*-axis which pierces the dot through its center and is perpendicular to the plane of the wetting layerrepresents a symmetry axis for the system.

In the presence of a hydrogenic impurity and under magnetic fields, the Hamiltonian of the system is given by

$$H_0 = \frac{1}{2m*}\left(\vec{p} + e\vec{A}\right)^2 + V(x,y,z) - \frac{e^2}{4\pi\varepsilon_0\varepsilon_r\left|\vec{r} - \vec{r}_i\right|} \tag{6.1}$$

where

$$m^*(x,y,z) = \begin{cases} m^*_{InAs}, & in \quad QD \\ m^*_{GaAs}, & in \quad exterior \end{cases} \tag{6.2}$$

is the effective mass, and

$$V(x,y,z) = \begin{cases} 0, & \text{in QD} \\ \Delta E_{\text{c}}, & \text{elsewhere} \end{cases} \tag{6.3}$$

is the potential energy. ΔE_c is the conduction band offset between the InAs and GaAs and the last term in Eq. (4.1) is the Coulomb interaction between the electron and the hydrogenic donor located at $\vec{r}_i$. We assume a vertical magnetic field $\vec{B} = B\hat{z}$ (Figure 6.1.).

Using the Coulomb gauge $\vec{A} = (B/2)(-y\hat{x} + x\hat{y})$, the Hamiltonian becomes:

$$\hat{H} = \frac{\hat{p}_x^2 + \hat{p}_y^2 + \hat{p}_z^2}{2m*} + \frac{eB}{2m*}\left(y\hat{p}_x - x\hat{p}_y\right) + \frac{e^2B^2}{8m*}\left(x^2 + y^2\right) + V(x,y,z) - \frac{e^2}{4\pi\varepsilon_0\,\varepsilon_r\left|\vec{r} - \vec{r}_i\right|}. \tag{6.4}$$

For low *B*, the magnetic confinement is much weaker than the geometric confinement and the diamagnetic term can be treated as a perturbation. In this case, the shift for the ground state energy of the impurity donor is given by

$$\Delta E = E(B) - E(B=0) = \beta B^2. \tag{6.5}$$

where:

$$\beta = \frac{e^2}{8m^*}\left\langle \rho^2 \right\rangle \tag{6.6}$$

is the low field diamagnetic susceptibility [38], [39] :
and

$$\left\langle \rho^2 \right\rangle = \left\langle x^2 + y^2 \right\rangle \tag{6.7}$$

is the mean square electron position in the plane perpendicular to the magnetic field.

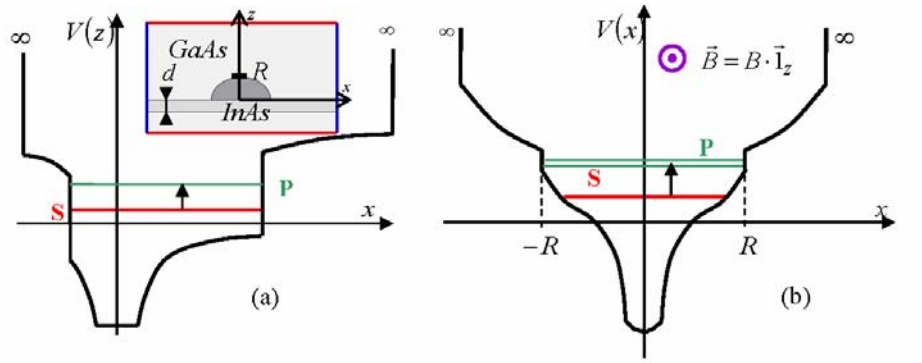

Figure 6.1. *Confinement potential including the Coulomb interaction associated to on-center impurity for InAs/GaAs QD without (a) and with applied magnetic field (b). Inset is a sketch of the InAs QD with its WL (darker gray) imbedded in a GaAs matrix (light gray).*

As the hydrogenic impurity behaves like an exciton with infinite hole effective mass, it is expected as the relation:

$$\Delta E = \frac{\beta B^2}{1 + \alpha B} \tag{6.8}$$

proposed in Ref. [38] for the diamagnetic shift of the exciton energy to be also a good approximation for the ground-state energy of the donor. Taking α and β as fitting parameters we check the validity of this dependence (which interpolates between the small and large magnetic field behavior), for on-center or on-surface impurities in dome-shaped InAs/GaAs QD.

6.3. Results and discussion

The input parameters for a typical InAs/GaAs QD are: $m^*_{\mathrm{InAs}} = 0.04\, m_0$, $m^*_{\mathrm{GaAs}} = 0.067\, m_0$ where m_0 is the free electron mass, $\Delta E_c = 500\ \mathrm{meV}$ [29] , $\varepsilon_r = 14.55$ [40].

In the following, I will choose for presentation some of the most relevant figures on the electronic properties of a donor impurity located on the surface or in the center of a self-assembled quantum point in InGaAs / GaAs, under the action of an external magnetic field, and the obvious conclusions specific to each chosen graph

Figure 6.2 presents the dependence of the lowest three energy levels and the corresponding probability of finding the electron inside the dome versus the magnetic field in the absence of the donor impurity.

For the ground state (Figure 6.2 a) we observe a weak change of the energies at low fields and a pronounced enhancement at higher fields. As B increases, the energy level starts showing a mixed behavior between spatial and magnetic confinement and, for large enough strengths, the ground state energy shows a linear dependence due to the formation of Landau levels.

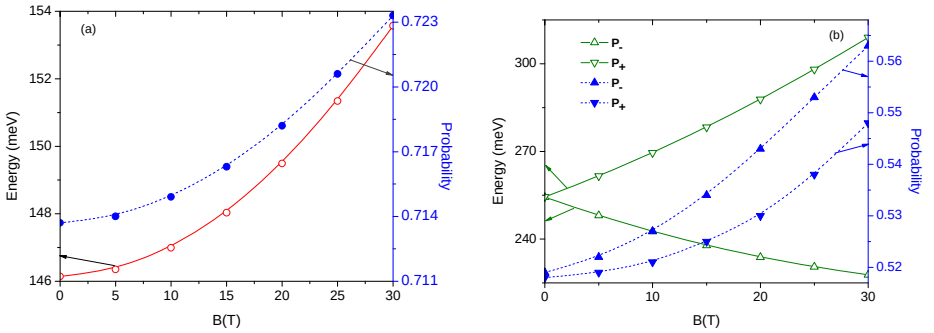

Figure. 6.2. *The energy levels (continuous lines, left scale) and the probability of finding the electron inside the dome (dashed lines, right scale) versus the magnetic field: (a) S – state; (b)* P_- *,and* P_+ *states, respectively. Results are for a QD without impurity.*

For the excited states, at a given magnetic field, the energy values depend on the sign of the azimuthal quantum number *m*. This dependence yields the simultaneous formation of blueshifted ($m > 0$) and redshifted ($m < 0$) states. As shown in Figure 6.2(b), the magnetic field removes the degeneracy of the first excited state corresponding to $m = \pm 1$, leading to P_+ and P_- states, respectively.

Figure 6.2 also shows the probability of finding the electron inside the dome for S- and P-states with varying magnetic field. With increasing of *B*, the electron cloud becomes more confined inside the dot, indicating the supplementary confinement induced by the magnetic field.

The results presented in Figure 6.4 correspond to the electron-impurity energies versus the magnetic field for different positions (on-center or on-surface) of the donor atom. In the present calculations, the cartesian coordinates of the on-center, top, and side impurities are (0, 0, 0), (0, 0, R), and (R, 0, 0), respectively.

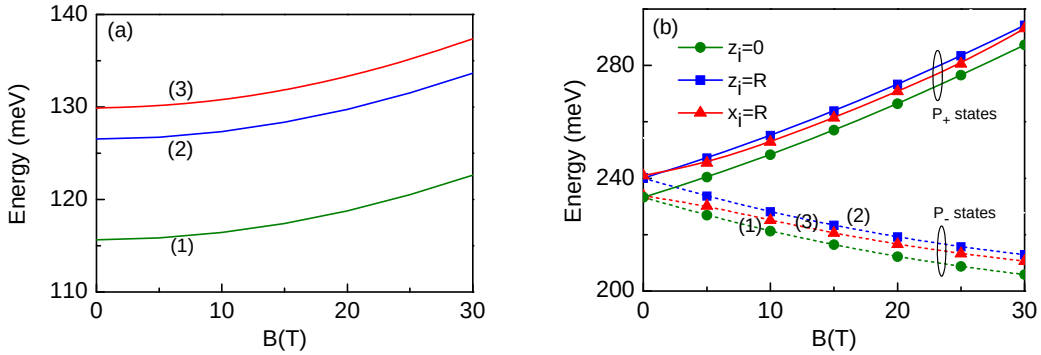

Figure 6.4. *Hydrogenic impurity energies in an InAs/GaAs dome shaped QD versus magnetic field. (a) Ground state; (b) first two excited states. Notations (1), (2) stand for on z-axis impurity positions with zi = 0, and zi = R where (3) is for the radial impurity position* $\vec{r}_i = (R,0,0)$*, respectively.*

As expected, the main effect of the impurity presence consists in the decrease of all energies because of the Coulomb interaction. For *zi = 0*, the small electron-impurity distance determines an increasing in the donor binding energy and consequently, a decreasing of the energy levels.

Figure 6.11 presents the lowest transition energies as a function of the magnetic field for different impurity positions within the QD. For comparison, the case of the structure without impurity is also shown.

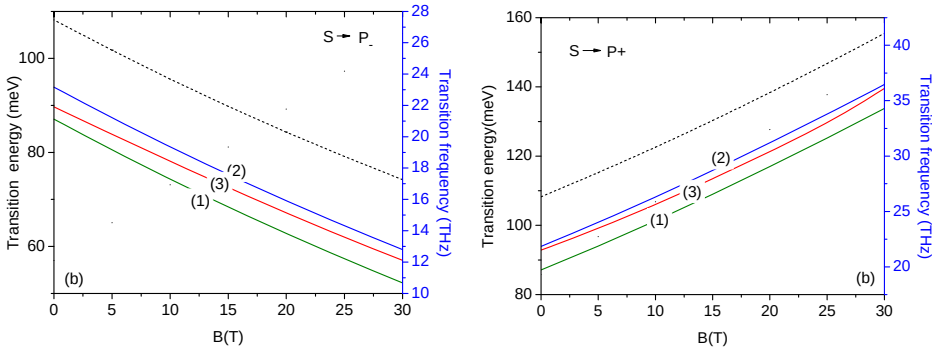

Figura 6.11. *Transition energy (frequency) for (a) $S \to P_-$ and (b) $S \to P_+$ transition as a function of magnetic field. Dashed lines are the results for a QD without impurity. Different impurity positions (the same as in Figure.6.4) are considered*

For $S \to P_-$ transition (which is the main optical transition in QDs [37,44]), we observe a linear decrease with *B* and, for all cases investigated, the theoretical curves have the same slopes (Figure 6.11a). The explanation for such a behavior would readily come from observing the variation of the involved energies shown in Figure 6.4. The corresponding transition frequencies ranging in the terahertz region and move towards the lower frequencies with increasing the magnetic field. The transition $S \to P_+$ could also happen under a y-polarized probe field [37], and, consistent with the results shown in Figure 6.4, it exhibits a linear increase of the transition energies (and related frequencies) as increasing the values of magnetic field (Fig. 11(b)).

Comparing these results with those for an impurity-free dome-shaped QD (dashed curves in Figure 6.11) one finds that electron-impurity potentials cause the shift the $S \to P_+$ and $S \to P_-$ frequencies towards lower THz values.

6.4. Conclusions

Using the finite element method, the effect of magnetic fields on the donor states and transition energies in a InAs/GaAs quantum dot coupled to its wetting layers is investigated. Results are obtained for different impurity locations. We found that the diamagnetic shift of the ground state energy increases monotonously with the applied field and can be described by a simple function which interpolates between the low and high magnetic-field behavior. Frequencies associated to the transitions between the S-like ground state and P_- (P_+) excited states range in terahertz region and show a magnetic field induced red (blue) shift, irrespectively of the impurity position.

6.5. Selective bibliography

[26] D. Bejan, "*Impurity-related nonlinear optical rectification in double quantum dot under electric field* ",Phys. Lett. A 380 (2016) 3836.
[27] D. Bejan, E. C. Niculescu, "*Intense laser effects on the optical properties of asymmetric GaAs double quantum dots under applied electric field*",Eur. Phys. J. B (2016) 89.
[28] K. Boz, B. Nisanci, S. Aktas, S. Erol Okan, "*Energy levels of GaAs/AlxGa1-xAs/AlAs spherical quantum dot with an impurity*", Appl. Surf. Sci. 387 (2016) 76.

[29] C.A. Duque, E. Kasapoglu, S. Sakiroglu, H. Sari, I. Sökmen, *"Intense laser effects on donor impurity in a cylindrical single and vertically coupled quantum dots under combined effects of hydrostatic pressure and applied electric field"*, Appl. Surf. Sci. 256 (2010) 7406.
[30] E. C. Niculescu, M. Cristea, A. Radu, "*Tuning a conventional quantum well laser by nonresonant laser field dressing of the active layer*",Superlattices Micro. 69 (2014) 65.
[31] J. Ganguly, S. Saha, S. Pal, M. Ghosh, "*Fabricating third-order nonlinear optical susceptibility of impurity doped quantum dots in the presence of Gaussian white noise*",Optics Comm. 363 (2016) 47.
[32] B. Çakır, Y. Yakar, A. Özmen, *"Linear and nonlinear optical absorption coefficients and binding energy of a spherical quantum dot"* Physica B 510 (2017) 86.
[33] M.G. Barseghyan, *"Energy levels and far-infrared optical absorption of impurity doped semiconductor nanorings: Intense laser and electric fields effects"*,Chemical Physics 479 (2016) .
[34] A. Talbi, E. Feddi, A. Oukerroum, E. Assaid, F. Dujardin, M. Addou, *"Photoionization cross section and binding energy of single dopant in hollow cylindrical core/shell quantum dot"*,Superlattices Microstruct., 85 (2015), 581.
[37] Sabaeian, M Riyahi, Physica E: *"Low-dimensional Systems and Nanostructures",* Physica E 89 (2017) 105.
[40] M. Dezhkam, A. Zakery, "*Electronic properties of hemispherical quantum dot/wetting layer with and without hydrogenic donor impurity", Physica B 443 (2014) 70.*

Chapter 7

Optical non-linearities associated to hydrogenic impurities in InAs/GaAs self-assembled quantum dots under applied electric fields

The results presented in this chapter were published in ***Philosophical Magazine vol 97 no. 35 (2017).***

7.1 Introduction

In this chapter, we present donor impurity-related non-linear absorption and non-linear optical rectification in an InAs/GaAs dome-shaped quantum dot (QD) with wetting layer (WL) under applied electric fields.

7.2. Theory

In this study, a dome-shaped InAs/GaAs QD with radius R = 7 nm grown on a 2 nm wetting layer is considered (see inset of Fig. 1a). The z axis is chosen to be perpendicular to the plane of the wetting layer.

In the presence of a hydrogenic impurity and under applied electric fields parallel to the zdirection the Hamiltonian of the system is given by:

$$H = -\frac{\hbar^2}{2}\nabla\frac{1}{m^*(x,y,z)}\nabla + V(x,y,z) + eFz - \frac{Z e_0^2}{\varepsilon_r\sqrt{x^2+y^2+(z-z_i)^2+d_{cutoff}^2}} \qquad (7.1)$$

where the significance of the sizes is the same as in Chapter 6, and $d_{cuttoff} = R\sqrt{10^{-5}}$

Following the theoretical framework of Paspalakis et al. [39], the total non-linear absorption coefficient for a transition between two levels $Ei = \hbar\omega i$ and $Ej = \hbar\omega j$, can be written as:

$$\alpha_{ij}(\omega) = \frac{\omega N \mu_{ij}^2 T_2}{\varepsilon_0 \hbar c n_r} \frac{\left| J_0^2\left(\frac{|\mu_{jj} - \mu_{ii}|E_0}{\hbar\omega}\right) - J_2^2\left(\frac{|\mu_{jj} - \mu_{ii}|E_0}{\hbar\omega}\right)\right|}{1 + T_2^2(\omega - \omega_{ji})^2 + \bar{\mu}_{ij}^2 E_0^2 T_1 T_2 / \hbar^2} \tag{7.4}$$

where

$$\bar{\mu}_{ij} = \mu_{ij}\left(J_0\left(\frac{|\mu_{jj} - \mu_{ii}|E_0}{\hbar\omega}\right) + J_2\left(\frac{|\mu_{jj} - \mu_{ii}|E_0}{\hbar\omega}\right)\right) \tag{7.5}$$

In Equations (7.4) and (7.5), $\omega_{ji} = (E_j - E_i)/\hbar$, J_0, J_2 are the ordinary Bessel functions of order 0 and 2, N is the electron density, T_1 is the population decay time and T_2 is the dephasing time. E_0 is the amplitude of the electric field $E(t) = E_0 \cos(\omega t)$ related to the incident intensity I_0 of the probe field by $I_0 = \frac{\varepsilon_0 c n_r E_0^2}{2}$ where ε_0 is the vacuum dielectric permittivity, n_r is the refractive index and c the vacuum speed of light. μij are the matrix elements of the dipole moment $\mu_{ij} = e\langle\Psi_i|\vec{\xi}\cdot\vec{r}|\Psi_j\rangle$ with $\vec{\xi}$ the incident light wave polarisation vector. We have considered the cases when the polarisation vector is directed in xOz plane (in-plane polarisation) or along the z-axis (z-polarisation).

The relative refractive index change (RIC) is given by [6]:

$$\frac{\Delta n(\omega)}{n_r} = -\frac{N\mu_{12}^2 T_2^2(\omega - \omega_{21})}{2\varepsilon_0 \hbar n_r^2} \frac{\left(J_0\left(\frac{|\mu_{22} - \mu_{11}|E_0}{\hbar\omega}\right) + J_2\left(\frac{|\mu_{22} - \mu_{11}|E_0}{\hbar\omega}\right)\right)^2}{1 + T_2^2(\omega - \omega_{21})^2 + \bar{\mu}_{12}^2 E_0^2 T_1 T_2 / \hbar^2} \tag{7.6}$$

In the same compact density-matrix formalism [39], the non-linear optical response (NOR) corresponding to an interlevels $i \rightarrow j$ transition can be written as:

$$\chi_0^{ij}(\omega) = \frac{2N|\mu_{jj} - \mu_{ii}|\mu_{ij}^2 T_1 T_2}{\varepsilon_0 \hbar^2} \frac{\left(J_0\left(\frac{|\mu_{jj} - \mu_{ii}|E_0}{\hbar\omega}\right) + J_2\left(\frac{|\mu_{jj} - \mu_{ii}|E_0}{\hbar\omega}\right)\right)^2}{1 + T_2^2(\omega - \omega_{ji})^2 + \bar{\mu}_{ij}^2 E_0^2 T_1 T_2 / \hbar^2} \tag{7.7}$$

7.3. Results and discussion

The parameters used in our calculations are: $N = 3\times10^{22}$ m^{-3}, the refractive index of the semiconductor $n_r = 3.55$, $T_1 = 1$ ps and T_2= 0.2 ps [42].

7.3.1. Electronic properties

In Figures 7.4. and 7.5., we have depicted some results of the calculation that will help to explain the characteristics of the optical properties under study: the transition (Figure7.4.), the off-diagonal interlevel matrix elements (Figure 7.5.(a)) and the difference of the diagonal matrix elements (Figure 7.5.(b)) as function of the applied electric field.

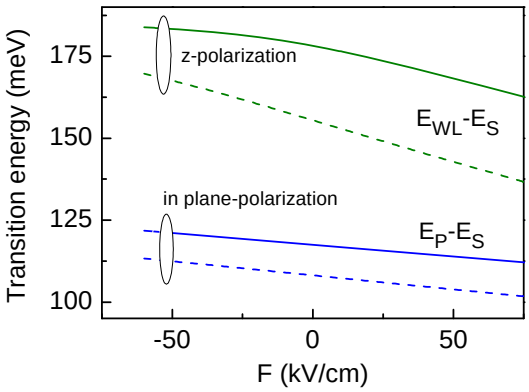

Figure 7.4. *Transition energies between the ground and the first excited states in a dome-shaped InAs/GaAs QD as a function of the applied electric field. Note: Solid and dashed lines refer to Z = 1 and Z = 0 cases, respectively*

As Figure 7.4 shows, the electric field results in a decrease of the transition energies, which will be evidenced by the red-shift in the resonant peaks of NOA and NOR. We observe that for both cases of incident light polarisations the transition energies are reduced as F increases due to a diminishing in the confinement of the carriers.

In Figure 7.5 we represented the dependence of the matrix elements on the electric field intensity.

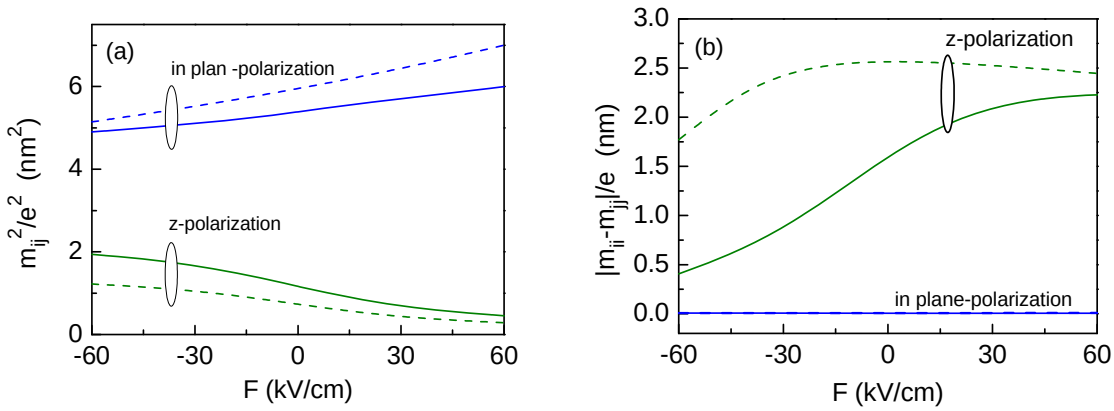

Figure 7.5 *(a) Square of the interlevel matrix elements and (b) the difference of the diagonal matrix elements in an InAs/GaAs QD as functions of the applied electric field. Note: Solid and dashed lines refer to Z = 1 and Z = 0 cases*

The dependence of the dipole matrix elements on the field strengths presented in Figure 7.5 can be explained observing the change in the spatial distribution of the involved wave functions discussed above. In a polarised QD, with growing the bias voltage the matrix element $\mu_{S\to P}$ (associated with in-plane polarised incident light) augments, whereas $\mu_{S\to WL}$ (associated with z-polarised incident light) diminishes.

In the impurity presence, the displacement of the ground state WF to lower z-values gives rise to the small (large) values of the matrix element $\mu_{S\to P}\mu_{S\to WL}$ observed in Figure 7.5(a) (solid lines).

7.3.2. Optical properties

The dependence of the optical properties – absorption coefficient, refractive index change and optical rectification – on the probe field energy is represented in Figure 7.6. for $Z = 1$ and different intensities I_0.

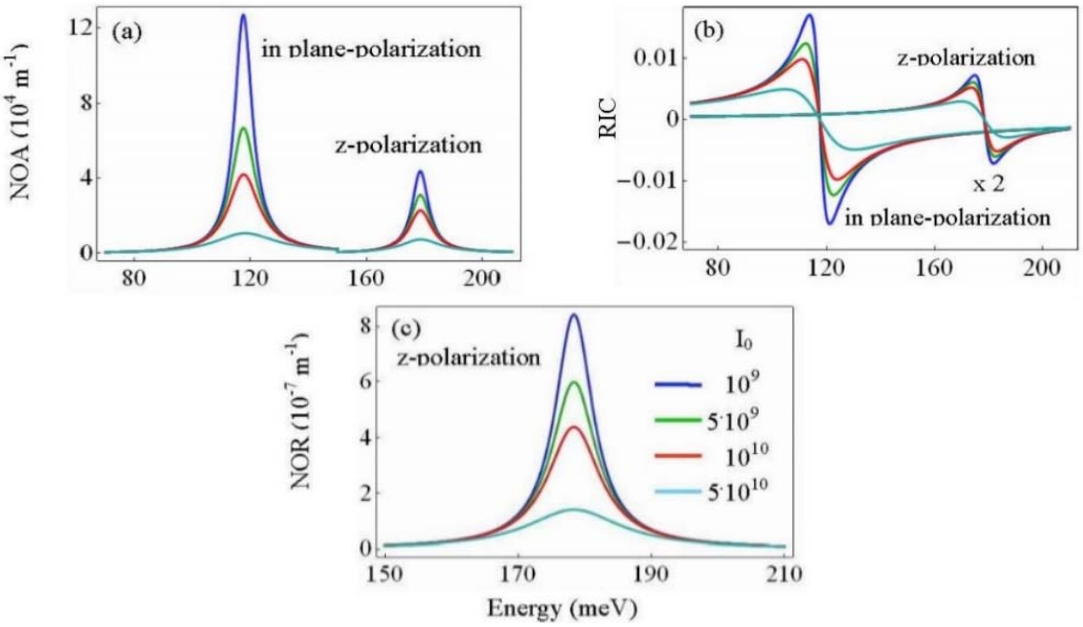

Figure 7.6 *(a) The non-linear absorption coefficient, (b) the refractive index change and (c) the non-linear optical rectification vs. the photon energy at four different probe field intensities. Note: The results are for Z = 1 and F = 0.*

In agreement with the results reported for an asymmetric one-dimensional double-well confining potential under a strong probe field excitation [39] we found that: (i) whereas in the weak and intermediate intensity regions the optical coefficients exhibit a linear intensity dependence, in the stronger intensity region this dependence becomes markedly non-linear; (ii) the absorption coefficient is always positive and the slope of the refractive index near resonance kept its negative sign, independent of the value of the field intensity.

In Figure 7.7, we present the intraband optical absorption coefficient as a function of the incident photon energy for several values of the electric field strength in a QD with (solid lines) and without (dashed lines) donor impurity.

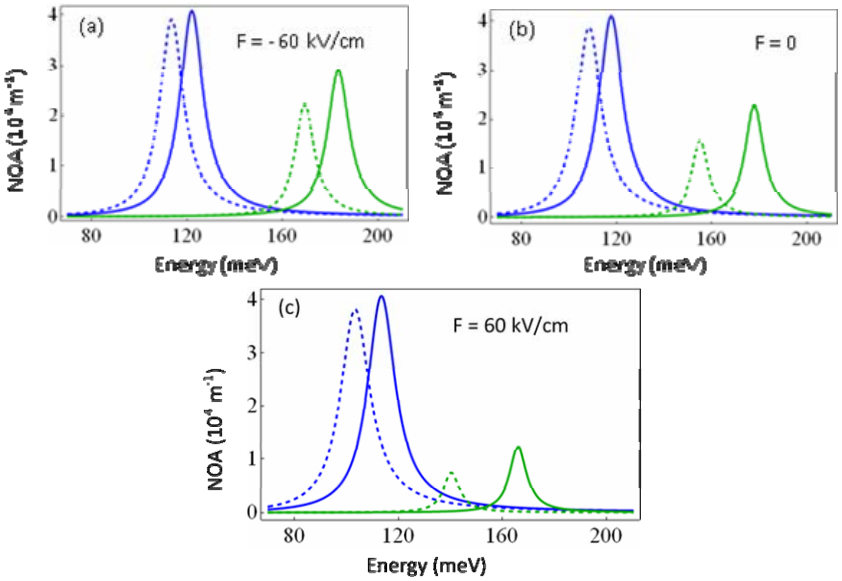

Figure 7.7*. Dependence of the non-linear absorption coefficient on incident photon energy at different electric field strength. The results are presented for in-plane polarization (blue curves) and z-polarization (green curves) of the incident light. Note: Solid and dashed lines refer to Z = 1 and Z = 0 cases, respectively.*

Comparing the absorption spectra for cases with and without impurity we note that: (i) the blueshift induced by the Coulomb term is enhanced as long as F augments because the S → WL transition energy exhibits a significant growth with electric field in comparison to the ones in the free-impurity QD; (ii) although falls markedly in amplitude when *F* increases, the NOA peak for the case with impurity remains higher than those associated with *Z = 0* case, for any field considered. This is related to increased values of the product $\omega_{ij}\,\mu_{ij}^2$ due to the electron-impurity attraction.

As NOA is strongly dependent on the probe field intensity, in Figure 7.8 this dependence is plotted in the case of exact resonance $\omega = \omega ij$ for both in-plane and z-polarised incident light. Three values of the applied electric field are considered.

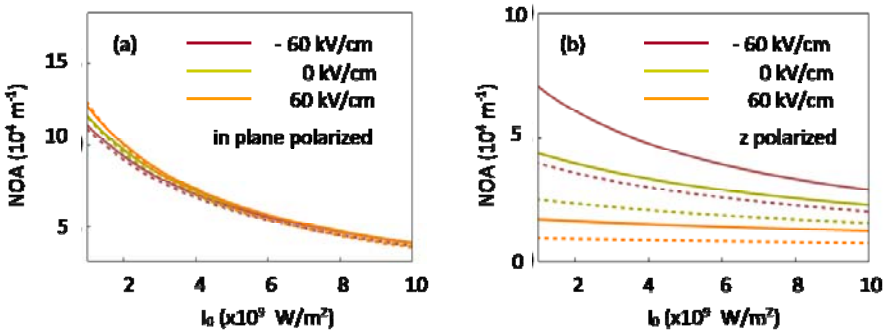

Figure 7.8. *Resonant peak values of the NOA as a function of the incident photon energy for several values of the applied electric field.*

We see that for in-plane polarised incident radiation (Figure 7.8(a)) NOA is nearly the same for cases with and without impurity and practically a F-independent quantity. On the other hand, the impurity presence is responsible for the increasing in the intensity of the NOA resonant peak for S-to-WL transition (see Figure 7.8(b)), more pronounced for negative applied fields and lower illumination intensities.

7.4 Conclusions

Within the effective mass approximation the electron states in a dome-shaped InAs/GaAs QD are calculated by means of the finite element method. The effects of WL, donor impurity and externally applied electric fields are also taken into account. The calculation allows to determine the transition energies from the ground state to the lowest excited ones as well as the corresponding dipole moment matrix elements. These quantities are used to investigate the features of the optical properties of the system under a strong probe field excitation. The non-linear optical absorption, relative refractive index change and non-linear optical rectification associated with interlevel transitions are calculated under a strong probe field excitation for both in-plane and z-polarisation of the incident light. According to our results as the electric field increases the absorption and dispersion peaks decrease and exhibit red shift. Hydrogenic impurity located at the origin induces a blue shift in the optical responses. For the optical absorption coefficient the peaks magnitude is enhanced by the impurity presence independent of the electric field strengths, whereas the non-linear optical rectification is larger in the case with impurity only for zero applied electric field.

7.5 Selective bibliography

[6] D. Bejan, "*Exciton effects on the nonlinear optical properties of semiparabolic quantum dot under electric field"*, Eur. Phys. J. Plus 132 (2017), p. 102.
[27] J.-Z. Zhang and I. Galbraith, *I"ntraband absorption for InAs/GaAs quantum dot infrared photodetectors",* Appl. Phys. Lett. 84 (2004), p. 1934–1936.
[28] T.A. Ameen and Y.M. El-Batawy, "*Polarization dependence of absorption by bound electrons in self-assembled quantum dots*", J. Appl. Phys. 113 (2013), p. 193102.
[39] E. Paspalakis, J. Boviatsis, and S. Baskoutas, "*Effects of probe field intensity in nonlinear optical processes in asymmetric semiconductor quantum dots"*, J. Appl. Phys. 114 (2013), p. 153107.

Conclusions

In this thesis we proposed a theoretical study on the electronic and optical properties of semiconductor nanostructures and the possibility of adjusting them by an appropriate modification of external fields - electric, magnetic, non-resonant laser radiation of high intensity - but also by the asymmetry of confinement potential. obtained by geometry or by the presence and position of impurity atoms.

For this, we conducted a literature study that aimed to present the main numerical methods used to calculate the electronic structure of nanostructures and synthesize information on the types of zero-dimensional systems with applications in optoelectronics.

Based on this study, we chose as objectives of the research **the phenomenon of electromagnetically induced transparency** - chapters 3 and 4, **the effects of external fields on the properties of GaAs / AlGaAs quantum rings** - chapters 4 and 5, and **optical properties of self-assembled quantum dots residual layer** - chapters 6 and 7. Furthermore, the numerical results were obtained in the approximation of the effective mass.

Electromagnetically induced transparency

For the ***GaAs / AlxGa1-xAs semi-parabolic quantum well*** :

- it has been shown that increasing the intensity of the non-resonant laser increases the width of the transparency window, while increasing the intensity of the electric or magnetic field the transparency window for absorbing the sample radiation is moved to higher energies.
- it has been pointed to obtaining of an optimal of the characteristics of the transparency induced by an adequate choice of the applied external fields.

For ***quantum rings with pseudoharmonic potential*** in impure GaAs, the possibility of switching the level structure in which the EIT appears from a Λ -type configuration to a scale-type configuration has been demonstrated, switching induced by the external magnetic field.

For both configurations, the following were observed:

- increased intervals for the transparency window and for the sub- (super-) luminal propagation domains when the magnetic field strength increases.
- modulation of the optical characteristics of the sample radiation - absorption coefficient, refractive index and group index - through the parameters of control radiation - intensity, Rabi frequency and phase shift.
- reduction of maxima for AC, RF and GI and a red-shift of the transparency window when the impurity moves from the minimum position of the confinement potential to the repulsive barrier of the structure.
- significant decrease of the critical field of the control radiation at which the EIT appears, reduction induced by the increase of the applied magnetic field.

GaAs quantum rings with a non-centric donor impurity

- the influence of the magnetic field on the probability of localization probability of the electron in the structure was highlighted, which determines the moments of dipole transition.
- the effects of increasing the magnetic field and moving the impurity position towards the outer radius of the ring on the electronic energy levels were studied.
- in the radial electric field, it has been shown that for moderate intensities the Stark displacement has a linear dependence on this parameter, while the polarizability of the impurity tends rapidly towards the saturation value.
- the dependence of the oscillator strength associated with the transitions between the impurity levels on the polarization of the incident light and on the position of the impurity inside the structure was analyzed. It was found that for the impurity placed in the direction of the electric field, the intensity of the transitions induced by the *y*-polarized light is at least an order of magnitude greater than that corresponding to an *x*-polarization.In contrast, for impurities located in the direction perpendicular to the field, the oscillator strength has appreciable values for *x*-polarized light.

Self-assembled hemispherical quantum dots with WL

- we observed a monotonous increase with the field applied for the diamagnetic displacement of the energy of the ground state.
- we proposed a simple analytical function that interpolates between the response to low and high - intensity magnetic fields for the energy dependence of the fundamental state of the donor impurity at the quantum point on the magnetic field.
- we calculated the frequencies associated with the transitions between the fundamental state of type S and the excited states of type P_- (P_+) and we observed a movement towards red (blue) induced by the magnetic field, regardless of impurity position.

- we studied the effects of a radial electric field on nonlinear optical processes in structures with and without impurity. It has been shown that in the presence of a central donor impurity, the values for NOA and RIC increase and the resonance maxima move to higher energy values.
- we have shown that while NOA and RIC can be observed both for an incident light polarized in the plane and for polarization after z, NOR cancels out for a polarized radiation in the plane. Another interesting result is that the maximum resonance of the NOR depends significantly on the light intensity and the intensity of the electric field.

The results of these studies have been published in prestigious international journals such as "Philosophical Magazine", "Chemical Physics", "European Physical Journal B", but also in "Romanian Reports in Physics".

2. Future perspectives

The studies performed can continue through the theoretical investigation of the effects of high - intensity laser radiation on the energy spectrum of quantum rings, for which a number of interesting results have been presented in the literature.

Various geometries will be included - elliptical, centric or non-centric rings, double rings with impurities in various positions, which offer the possibility to continue the research by studying new characteristic properties.

APPENDIX I:

List of scientific publications published during the doctoral thesis

Articles published in ISI-WOS indexed journals:

1. Ecaterina C. Niculescu, Cristina Stan, Gabriela Tiriba, **Cristina Trușcă** "Magnetic field control of absorption coefficient and group index in an impurity doped quantum disc ", "The European Physical Journal B" (2017), DOI: 10.1140/epjb/e2017-80138-0, revistă cotată ISI, **factor de impact IF=1.44, AIS=0.449**

2. Mihail Cristea, Ecaterina C. Niculescu, **Cristina Trușcă** "Optical nonlinearities associated to hydrogenic impurities in InAs/GaAs self-assembled quantum dots under applied electric fields", Philosophical Magazine vol 97, nr. 35 (2017) DOI:10.1080/14786435.2017.1381775 , revistă cotată ISI, **factor de impact IF=1.885, AIS =0.535**

3. Ecaterina C. Niculescu, Cristina Stan , Mihail Cristea, **Cristina Trușcă** "Magnetic-field dependence of the impurity states in a dome-shaped quantum dot", Chemical Physics, volum 493, pag. 32-41, (2017)**,** doi.org/10.1016/j.chemphys.2017.06.004, **revistă cotată ISI, factor de impact IF=1.707 , AIS =0.464**

4. **Cristina Trușcă**, Cristina Stan, Ecaterina C. Niculescu, "Stark Shift and oscillator strenghts in a GaAs quantum ring with off-center donor impurity", U.P.B. Sci. Bull., Series A, Vol. 80, Iss. 1, (2018), ISSN 1223-7027, **factor de impact IF=0.478,**

AIS =0.094

5. Doinița Bejan , **Cristina Trușcă** "Effects of electric, magnetic and intense laser fields on the electromagnetically induced transparency in a semiparabolic quantum well", Rev. "Romanian Reports in Physics", vol. 70, pag.412 (2018), revistă cotată ISI, **factor de impact IF=1.940 , AIS=0.296**

Scientific conferences

Doina Bejan**, Cristina Trușcă** "Effect of electric,magnetic and intense laser fields on the electromagnetically induced transparency in a semi-parabolic quantum well", "Annual Scientific Conference Knowledge means Physics", University of Bucharest, Faculty of Phisics, Bucharest, Romania, 23-24 iunie 2017